

CURRENT-SHEET FORMATION in RELAXING PLASMAS

INHIBITING ACTION OF α -EFFECT

Report on Research Contract, Ref. EMR 470 M, U.K.A.E.A.

K. Bajer and H.K. Moffatt

Department of Applied Mathematics and Theoretical Physics

Silver Street, Cambridge CB3 9EW

The influence of the α -effect on two-dimensional relaxation in a cylindrical geometry is examined. The α -effect, like Ohmic dissipation, breaks the topological constraints of ideal MHD. Hence it may have a dramatic effect.

1. Introduction

Browning et al's (1987) computations of fields \mathbf{B} satisfying the force-free condition $\nabla \times \mathbf{B} = \mu \mathbf{B}$ with $\nabla \mu = 0$ show the existence of an X-point in the entry region of a spheromak. This suggests that the relaxed state in the real device contains either an X-point or a current-sheet with corresponding topology. The latter is likely to be formed in a process of X-point collapse, especially if the final steady state is not completely force-free.

The evolution of a plasma towards the quasi-steady state that fusion experiments try to achieve is a combination of different phenomena generally called 'relaxation'. The term covers two conceptually different but experimentally inseparable stages of evolution towards equilibrium. First the large scale magnetic fields evolve under the influence of their own Lorentz force until this becomes potential, and can therefore be balanced by the pressure gradient (Moffatt 1985). In a perfectly conducting medium this would be the final state, further evolution being prevented by topological constraints. Second, in real plasmas the topological constraints may be broken and the magnetic field can further lower its energy evolving towards a force-free state as described by Taylor (1974).

Although Ohmic diffusion is ultimately responsible for changes in the field topology, little is known about the dynamic processes enhancing this diffusion. One such process is the fast magnetic reconnection in current-sheets which are usually formed during the ideal phase

of relaxation (for a review see Priest 1985 and references therein; also Soward & Priest 1985). This is a local process and it is doubtful if it can sufficiently explain fast relaxation to a global force-free state.

Another much more complex mechanism of rearranging the magnetic flux is the local generation of large-scale magnetic fields by small-scale motions. The small-scale motions are induced either through the turbulent cascade from large-scale motions directly driven by the large-scale Lorentz force or by local phenomena like, say, strong heating in current sheets. Such small-scale turbulence may *locally* give a mean field dynamo action with the α -effect being its simplest manifestation.¹

The relaxing plasma, unlike the usual mean field dynamo, does not contain external energy sources driving the small-scale motions. The large-scale fields can be generated only locally and ultimately the energy for this local creation must be drawn from the potential energy of the field in some other part of the system.² Hence there is no net dynamo action in the relaxing plasma. Instead there are local spots of mean field creation. Such 'local dynamos' can change the field topology. The topological constraints are broken by a mechanism essentially different from simple reconnection. This local dynamo action changes the dynamics of the mean field and it is important to understand some basic dynamic events which take a different course when this type of α -effect operates. In previous studies (Bajer 1989) we have found that in the absence of any α -effect, relaxation in the neighbourhood of an X-type neutral point in general leads to the formation of a current sheet. In the present work, we find that, when an α -effect is included, this tendency to form current-sheets may be inhibited, the X-type neutral points being converted to O-type neutral points before the current-sheet can form.

¹ There is some evidence of the α -effect in the RFP (Gimblett & Watkins 1975).

² It is possible to relate α to \mathbf{B} in such a way that the total helicity is conserved and the total energy always decreases (Boozer 1986, Gimblett 1986).

2. Brief description of the code

We have developed a computer code simulating two-dimensional incompressible resistive MHD with α -effect in a cylindrical domain. The magnetic and velocity fields have all three components but they are independent of the cartesian coordinate z along the axis of the cylinder (the 'toroidal' direction). Hence we have:

$$\mathbf{B} = \left(\frac{\partial A}{\partial y}, -\frac{\partial A}{\partial x}, B \right) ; \mathbf{V} = \left(\frac{\partial \Psi}{\partial y}, -\frac{\partial \Psi}{\partial x}, V \right)$$

where $A(x, y)$, $\Psi(x, y)$ are flux- and stream-function of the poloidal parts, B_P , V_P ; and $B(x, y)$, $V(x, y)$ are toroidal components.

The α -effect, assumed non-isotropic, but isotropic in the poloidal plane, is parametrized by two coefficients: α_T and α_P :

$$\mathbf{E} + \mathbf{V} \wedge \mathbf{B} + \boldsymbol{\alpha} \cdot \mathbf{B} = \eta \mathbf{j} \quad \text{where} \quad \boldsymbol{\alpha} = \begin{pmatrix} \alpha_P & 0 & 0 \\ 0 & \alpha_P & 0 \\ 0 & 0 & \alpha_T \end{pmatrix}$$

(cf Moffatt 1978). The incompressible MHD equations are then:

$$\frac{\partial A}{\partial t} = \{\Psi, A\} + \alpha_T B + \eta \nabla^2 A, \quad (1a)$$

$$\frac{\partial B}{\partial t} = \{\Psi, B\} - \{A, V\} - \alpha_P \nabla^2 A - \nabla \alpha_P \cdot \nabla A + \eta \nabla^2 B, \quad (1b)$$

$$\frac{\partial V}{\partial t} = \{\Psi, V\} - \{A, B\} + \nu \nabla^2 V, \quad (1c)$$

$$\frac{\partial \omega}{\partial t} = \{\Psi, \omega\} + \{A, \nabla^2 A\} + \nu \nabla^2 \omega \quad (1d)$$

$$\omega = -\nabla^2 \Psi, \quad (1e)$$

where ω is the toroidal component of vorticity and $\{ , \}$ is the Jacobian, i.e. in polar coordinates:

$$\{f, g\} = \frac{1}{r} \left(\frac{\partial f}{\partial r} \frac{\partial g}{\partial \theta} - \frac{\partial f}{\partial \theta} \frac{\partial g}{\partial r} \right)$$

In the absence of the α -effect, the boundary conditions on the surface at a solid perfectly conducting boundary are:

$$\mathbf{U}|_{\partial D} = 0, \quad \mathbf{n} \cdot \mathbf{B}|_{\partial D} = 0, \quad \mathbf{n} \times \mathbf{E}|_{\partial D} = 0$$

Hence at a perfectly conducting cylindrical boundary $r = R$, we have:

$$\Psi|_{r=R} = 0, \quad \left. \frac{\partial \Psi}{\partial r} \right|_{r=R} = 0, \quad V|_{r=R} = 0.$$

$$\left. \frac{\partial A}{\partial \theta} \right|_{r=R} = 0, \quad \left. \frac{\partial A}{\partial t} \right|_{r=R} = 0, \quad \left. \frac{\partial B}{\partial r} \right|_{r=R} = 0.$$

In our computations we use a simplified passive boundary condition $B|_{r=R} = 0$ instead of constant toroidal flux, specified by $\left. \frac{\partial B}{\partial r} \right|_{r=R} = 0$. This condition holds for a boundary that is perfectly conducting in the z -direction, perfectly insulating in the θ -direction (as would be the case for a segmented boundary with slits parallel to the z -axis), and there is no external driving.

The α -effect introduces 'generation' terms in eqns. (1) which should vanish on the boundary. As $B|_{r=R} = 0$, this requirement does not impose any restrictions on α_T . Moreover, in the simulations performed so far, we took $\alpha_P = 0$ in the entire domain so the compatibility conditions at the boundary were satisfied identically³.

The code was written in such a way that α_T, α_P and both diffusion coefficients, viscosity ν and Ohmic diffusion η , could be functions of time and space. These are updated at every time step so it is easy also to make them functionally dependent on the magnetic field. This could be used to include such effects as the nonlinear saturation of the α -effect (see, e.g., Gilbert & Sulem 1990) even with a non-local relation between α and \mathbf{B} . The code is based on an explicit second-order finite-difference scheme on a uniform mesh in polar coordinates. To solve the Poisson equation for Ψ we use the fast Fourier transform

³ The α -effect can be calculated analytically in a model situation when the small-scale motions are helical waves propagating in the z -direction. In this case, one obtains $\alpha_P = 0$, $\alpha_T \neq 0$ (see Moffatt 1978, chap. 7).

in the angle variable and solve the one-dimensional boundary-value problem in the radial variable for each Fourier amplitude. The boundary conditions at $r = 0$ are determined from continuity and regularity of Ψ, A, B, V . The vorticity ω at $r = R$ is calculated by standard methods (Roache 1976, chap. III). The terms $\{A, \nabla^2 A\}$ and $\{\omega, \Psi\}$ can be easily evaluated when written in the conservative form:

$$\{A, \nabla^2 A\} = \frac{1}{r} \left[\frac{\partial}{\partial \theta} \left(\frac{\partial A}{\partial r} \nabla^2 A \right) - \frac{\partial}{\partial r} \left(\frac{\partial \Psi}{\partial \theta} \nabla^2 A \right) \right]$$

This form, when discretised, generally gives better results (Roache 1976, p. 32).

3. Numerical results

We have carried out three long simulations (see table 1 for the parameter values). In all cases ν, η and α_T were constant in time and space (with $\alpha_T = 1$) and $\alpha_P = 0$. The mesh size was 64×64 , the time-step $DT = 10^{-4}$ and $\eta = 10^{-3}$. Typical velocities were $\approx 10^{-1}$, so that the magnetic Reynolds number was in the range $10 < Rm < 100$ (the cylinder had unit radius). In all cases the evolution was followed from $t = 0$ to $t = 2.3 \div 2.8$. For a 64×64 mesh each time-step takes approximately 0.75s so each simulation took about 5 ÷ 6 hrs of computer time. The computation was carried out on the Cambridge University mainframe IBM 3084.

We tried two different initial conditions (fig. 1a,b). In both cases we had at $t = 0$, $\Psi = V = 0$, a non-equilibrium poloidal magnetic field with an X-type neutral line on the axis of the cylinder, and a toroidal magnetic field symmetric about $r = 0$:

$$A(t = 0) = r^2(1 - r^2)(S - \cos^2 \theta) \quad , \quad B(t = 0) = 1 - r^2 \quad .$$

The parameter S determines the angle α of the X-point. In runs I and II we had $S = 0.5$ which corresponds to $\alpha = 45^\circ$ and in run III $S = 0$, i.e. $\alpha = 90^\circ$. The data for these runs are shown in table 1. We know from previous work (Bajer 1989) that in the absence of the α -effect the initial condition $S = 0.5$ relaxes towards a stable equilibrium with a current-sheet being formed through the collapse of the X-point (see fig. 1c)⁴. Under the

⁴ When $\alpha_T = 0$ the toroidal components are passive (see eqns. 1) so they do not affect the dynamics of the poloidal field and flow.

same circumstances the initial condition with $S = 0$ tends to a stable equilibrium with a symmetric X-point ($\alpha = 90^\circ$) which shows no tendency to collapse (fig. 1d).

Here we investigate how the α -effect affects the relaxation process in these two situations.

Inhibition of current-sheet formation

The most obvious difference in all runs is the change of topology. For example, when $S = 0$, with $\alpha_T = 0$ the initial topology (fig. 2a) is preserved. With $\alpha_T \neq 0$ this topology is immediately changed in the manner shown in figure 2b; the topological constraints being broken, the separatrix can migrate towards the centre. In general, when $S \neq 0$, if the X-point collapse is slower than the shrinking of the central flux system (8 shaped) then the formation of the current-sheet is prevented. The sequence of contours of A , which coincide with lines of the poloidal part of the field, is shown in figure 3(a-d). The central neutral point changes from X-type to O-type and, at later times (figure 3d, $t = 2.28$), there is a roughly annular region of weak poloidal field surrounding it. The existence of this region which we call the 'flux gap' probably depends on the profile of B which in our case has its maximum at the centre.

Poloidal oscillations

When the magnetic X-point at $t = 0$ is not symmetric ($\alpha < 90^\circ, S \neq 0$) and therefore has a tendency to collapse, we find that a simple 'four-roll' poloidal flow develops with a stagnation point at the centre (fig. 4a). This flow pattern is a result of squeezing the fluid from between the two stronger magnetic eddies as they press against each other⁵ and this in fact persists for times $t \lesssim 3.1$ (for $S = 0.5$).

The toroidal field is advected by the stagnation point flow and the B -contours are rapidly deformed into ellipses elongated in the stretching direction of the flow (horizontal on our diagrams, fig. 4b). The α -effect constantly creates the poloidal field with A proportional to B , that is the field-lines coinciding with B -contours. Hence we obtain a very flat magnetic eddy at the centre.

⁵ The same happens when $\alpha_T = 0$.

Strong magnetic eddies in weaker ambient field are governed by the tendency to attain circular shape. It follows that the flat central eddy starts the 'four-roll' flow in the direction opposite to the original one (fig. 4d). This is the basic mechanism of what we call 'poloidal oscillations'⁶.

Fast flows induced by poloidal oscillations may become (2-D) turbulent (fig. 4e). Our low resolution computations can not be expected to be reliable when very small scales develop in the central region. However, they indicate that turbulence may have a damping effect on (largest scale) poloidal oscillations by mixing the toroidal field (fig. 4f)⁷. Poloidal oscillations will now be repeated in smaller scales 'feeding' on small-scale gradients of B . Therefore the α -effect, through the poloidal oscillations, greatly facilitates the excitation of smaller scales⁸. It is possible that in certain conditions such a process may bridge the scale separation on which the concept of the α -effect is based.

Toroidal oscillations

The advection of non-uniform B plays an essential role in the poloidal oscillations described above. The toroidal field, and therefore the poloidal current, can also be *created* from \mathbf{B}_P by the shearing flow in the z -direction. This gives a toroidal Lorentz force modifying the toroidal flow. There exists a particular mode of oscillation which is possible even with $B(t = 0) = 0$. In this mode B is entirely created by shearing of \mathbf{B}_P . In section 4 we show that poloidal motions are not essential for this mode and hence we call it 'toroidal oscillations'. These are not so easily identifiable in our numerical simulations as they are always mixed with the poloidal mode. In run III the latter is greatly reduced because of the symmetry of the initial condition (fig. 1b). Initial deformation of the B -contours in the central region is not dipolar but quadrupolar (fig. 6a) and hence there is no flat central magnetic eddy. Despite a much smaller viscosity the poloidal flow does not become turbulent (fig. 6f).

⁶ When viscous damping is small (Run II) the flat central eddy may break in two separate parts which then begin to oscillate (Fig. 5.)

⁷ Note that *gradients* of B are the sources of poloidal field (from the curl of eqn. 1a)

⁸ No turbulence was found in the computations with $\alpha = B = V = 0$ (Bajer 1989).

A clear manifestation of toroidal oscillations can be seen between $t = 0.6$ and $t = 1.0$. Comparing the B -contours (fig. 6a,b) we notice two regions of strong toroidal field above and below the central region. Advection of B by the persisting 'four-rolls' flow (figs. 6d,e) can not account for these two strong B regions. They are created from \mathbf{B}_P by the shearing toroidal flow (fig. 6g,h).

Further we can see several oscillations of this kind. For example at $t = 1.8$ (figs. 6c,i) we recognise a similar pattern rotated by 90° . It seems that these oscillations are generated in the central region and propagate outwards (fig. 6j). No precise measurements of their period were taken but it appears that the frequency increases with time. A plausible explanation for this increase is that, due to the α -effect, \mathbf{B}_P grows stronger and therefore becomes more 'rigid', i.e. it resists shearing with increasing strength.

4. Local solutions

Let us choose an arbitrary point in space for the origin of the cartesian coordinates. If $\alpha_P = \eta = \nu = 0$, the eqns. 1a-d admit local solutions. We can expand Ψ, V, ω, A and B in Taylor series in a small neighbourhood of the origin:

$$f(x, y) = \sum_{p=0}^{\infty} \sum_{q=0}^p f_{(p,q)}(t) x^p y^{p-q} .$$

Substituting this expansion in eqn. 1a-d we obtain an infinite system of coupled ODE's for the time evolution of the coefficients $\Psi_{p,q}(t)$, $V_{(p,q)}(t)$, $\omega_{(p,q)}(t)$, $A_{(p,q)}(t)$ and $B_{(p,q)}(t)$.

A crucial observation here is that the coefficients with $p = 0, 1, 2$, i.e. the terms which are constant, linear or quadratic in x, y , are coupled to the other terms only by diffusion, α_P and the boundary conditions on Ψ which are necessary to solve the Poisson equation. There is no coupling through the nonlinear terms. Hence, if $\alpha_P = 0$, the $p \leq 2$ terms evolve independently of other coefficients as long as diffusion and the influence of the boundary are negligible. In this case, the dynamics of the low-order terms, which dominate near the origin, gives us a particular kind of local solution of the equations 1a-d.

We have five relevant time-scales in the problem: two diffusive time-scales: T_η, T_ν ; two time-scales associated with the α -effect: $T_P \sim 1/\alpha_P$, $T_T \sim 1/\alpha_T$; and T_S - the time-scale

on which a given point ‘communicates’ with the boundary through magnetoacoustic and Alfvén waves. Local MHD solutions in the neighbourhood of a point may be expected to emulate the true dynamics for times smaller than T_η, T_ν, T_P and T_S . At the same time the toroidal α -effect is essential for the local solutions, so all the time-scales mentioned above must be longer than $T_T \sim 1/\alpha_T$. Clearly, in an incompressible fluid, pressure waves travel infinitely fast and therefore any point communicates instantaneously with the boundary unless the system is open in the sense that the boundary absorbs pressure waves. Hence, incompressible local solutions may be a good approximation in a compressible fluid far away from the boundary. There may also exist some particular local solutions for which the boundary conditions are not too important. Those are likely to be valid even in a strictly incompressible fluid. This is the case with toroidal oscillations.

We look for solutions of 1a-d with $\eta = \nu = \alpha_P = 0$ and such that Ψ, V, A and B are at most quadratic in x, y :

$$f(x, y, t) = f_0(t) + f_1(t)x + f_2(t)y + f_{11}(t)x^2 + f_{22}(t)y^2 + f_{12}(t)xy. \quad (4.1)$$

The local topology of the magnetic field near $(x, y) = (0, 0)$ is determined by the coefficients $A_1(t), A_2(t), B_0(t)$. When any A_1, A_2, B_0 are nonzero then the field has the topology of a bundle of parallel lines and for $A_1 = A_2 = B_0 = 0$ there is a neutral line at $x = y = 0$ (fig. 7).

In the rectilinear topology, local solutions are waves and they are found by Fourier rather than Taylor series expansion. Near a neutral line the field is not locally constant and therefore simple hydromagnetic waves are not valid local solutions. This is where the solutions of type (4.1) have the best chance of providing a good approximation to the full dynamics. For this reason we choose a subfamily of (4.1) with $A_1(t) = A_2(t) = B_0(t) = 0$. It follows from 1a-d that the linear terms of Ψ, V and B must also vanish⁹. This, in turn, implies that A_0, V_0, Ψ_0 are constant.

Solutions of the form (4.1) have uniform ‘toroidal’ vorticity. Hence the change in the

⁹ If, for example, $V_1(t) \neq 0$ then $\{A_{22}(t)y^2, V_1(t)x\} = -2A_{22}(t)V_1(t)y$. Then from 1b we have $\frac{\partial B_2(t)}{\partial t} \neq 0$ and eqn. 1a implies that a linear term in A will grow.

poloidal velocity is entirely due to the pressure which is determined by conditions on the boundary. Therefore the time evolution of Ψ is not determined locally and for the purpose of local solutions it has to be arbitrarily assumed. Here we make the simplest choice $\Psi = 0$. Other possibilities can also be of interest, e.g. a simple quadratic stagnation point flow could be chosen to model the influence of the X-point collapse on toroidal oscillations¹⁰.

We come to the conclusion that local dynamics near a neutral line are governed by the quadratic terms in A , B and V .

Equations 1a-d yield the following system of ODEs for the amplitudes of the quadratic terms:

$$\begin{aligned} \frac{dA_{11}}{dt} &= \alpha_T B_{11} , & \frac{dB_{11}}{dt} &= 2(A_{12}V_{11} - A_{11}V_{12}) \\ \frac{dA_{22}}{dt} &= \alpha_T B_{22} , & \frac{dB_{22}}{dt} &= 2(A_{22}V_{12} - A_{12}V_{22}) \\ \frac{dA_{12}}{dt} &= \alpha_T B_{12} , & \frac{dB_{12}}{dt} &= 4(A_{22}V_{11} - A_{11}V_{22}) \end{aligned} \quad (4.2)$$

$$\frac{dV_{11}}{dt} = 2(A_{12}B_{11} - A_{11}B_{12})$$

$$\frac{dV_{22}}{dt} = 2(A_{22}B_{12} - A_{12}B_{22})$$

$$\frac{dV_{12}}{dt} = 4(A_{22}B_{11} - A_{11}B_{22})$$

Eventually we would like to compare local solutions with the numerical simulations. The latter exhibited $x \rightarrow -x$ and $y \rightarrow -y$ symmetry so we choose a subsystem of (4.2) with

¹⁰ Arter (1986) considers a different set of exact MHD solutions obtained by Taylor series expansion. In his work both the velocity and the magnetic field are purely poloidal and *linear* in x and y . Hence the Lorentz force is potential and the non-trivial dynamics comes from the pressure-driven poloidal flow (see Arter 1986 and references therein). The local solutions we present here include *quadratic* $V(x, y)$ and $B(x, y)$ which are coupled to $A(x, y)$ by the α -effect while the poloidal flow does not play any part in the dynamics.

the same symmetries, i.e. $A_{12} = B_{12} = V_{11} = V_{22} = 0$:

$$\begin{aligned}
\frac{dA_1}{dt} &= \alpha_T B_1 \\
\frac{dA_2}{dt} &= \alpha_T B_2 \\
\frac{dB_1}{dt} &= -2A_1 V \\
\frac{dB_2}{dt} &= 2A_2 V \\
\frac{dV}{dt} &= 4(A_1 B_2 - A_2 B_1)
\end{aligned} \tag{4.3}$$

where $A_1 = A_{11}$, $A_2 = -A_{22}$, $B_1 = B_{11}$, $B_2 = -B_{22}$, $V = V_{12}$.

We can set $\alpha_T = 1$ by the following scaling:

$$t = \alpha_T^{-1} t^*, \quad A = \alpha_T A^*, \quad B = \alpha_T B^*, \quad V = \alpha_T V^* .$$

This means that $\alpha_T \rightarrow 0$ is a singular limit. When $\alpha_T = 0$ the system (4.3) is linear. Because of the singular character of the limit it becomes non-linear for any $\alpha_T \neq 0$ despite the fact that α_T multiplies linear terms.

Equations (4.3) have two families of fixed points:

- i) $A_1, A_2 = \text{const}, \quad V = 0, \quad B_1 = B_2 = 0,$
- ii) $A_1 = A_2 = 0, \quad V = \text{const}, \quad B_1 = B_2 = 0;$

and some simple solutions:

- a) $A_1 = B_1 = 0, \quad V = \text{const}, \quad \frac{d^2 A_2}{dt^2} = 2\alpha_T V A_2, \quad B_2 = \alpha_T^{-1} \frac{dA_2}{dt},$
 $\alpha_T V < 0$ (oscillations) , $\alpha_T V > 0$ (exponential growth);

- b) $A_1 = \alpha_T B_1 t + \tilde{A}_1, \quad A_2 = \alpha_T B_2 t + \tilde{A}_2, \quad V = 0$
 $\tilde{A}_2 B_1 - \tilde{A}_1 B_2 = 0, \quad \tilde{A}_1, \tilde{A}_2, B_1, B_2 = \text{const}.$

We also note the existence of an invariant:

$$V^2 + 4B_1B_2 = \text{const}$$

which does not have any obvious physical meaning.

Linearising (4.3) around a fixed point i) we find that small perturbations have a growth rate

$$\sigma = \pm 4\sqrt{A_1A_2} .$$

For an X-type neutral point at the origin we have $A_1A_2 > 0$ and exponential growth while for an O-point $A_1A_2 < 0$ and we have oscillations. Solving the non-linear system (4.3) we find similar behaviour.

In figure 8a we show V as a function of time for a solution with the initial condition $A_1 = -0.1$, $A_2 = 1$, $B_1 = B_2 = 0$, $V = 0.01$. There is now an O-point in the poloidal field and we find regular oscillations with no initial rapid growth. The period estimated from the diagram $T \approx 5$ is equal to the period $T = \pi/2\sqrt{A_1A_2}$ of small oscillations around a fixed point i).

In figure 8b we show $V(t)$ for a solution which differs only by the sign of $A_1(t = 0)$, i.e. at $t = 0$ it has an X-point at the origin. After a period of rapid exponential growth the regime of oscillations with increasing frequency and decreasing amplitude is established. The transition from exponential growth to oscillations occurs at $t \approx 4.5$. It coincides with the change of topology from X-point to O-point. To demonstrate this we have plotted $f = A_1/(A_1 + A_2)$ as a function of time (fig. 9). For an X-point with an angle θ we have $f = \cos^2 \theta$ while for an O-point f is a measure of its flatness. Hence $0 < f < 1$ corresponds to an X-point and $f < 0, f > 1$ to an O-point.

We notice in figure 9 that f changes sign at $t \approx 4.4$. This again is in agreement with linear theory which predicts exponential growth for an X-point and oscillations for an O-point. For later times $f(t)$ tends to a constant negative value, which means that asymptotically the system prefers a flat elliptical O-point. This was confirmed in many computations with different initial conditions both of X-type and O-type.

In figure 10 we show yet another solution with initial values $A_1 = 1$, $A_2 = 2$, $B_1 = 1$, $B_2 = -2$, $V = 0$. This time the solution cannot be regarded as a small perturbation of a fixed point (because $B_1, B_2 \neq 0$). Still it is qualitatively similar. We notice that the magnitude of A_1 and A_2 grows with time. Therefore the value of $|\sqrt{A_1 A_2}|$ grows too which explains the increasing frequency of the oscillations (stronger field becomes more 'rigid'). Such an increase was also found in the full dynamical simulations described earlier.

5. Conclusions and suggestions for further work

Simulations of mean field evolution have been carried out before, especially in studies of solar and stellar dynamos (cf e.g. Weiss 1989). So far attention has been focussed on the dynamo action in flows driven by non-magnetic forces. The main task of previous computations was to find and investigate the growth and maintenance of the magnetic field drawing its energy from the flow.

In the present work we have rather studied the influence of the α -effect on relaxation of a mean field originally far from equilibrium. The α -effect which is likely to occur at least locally provides a simple model of the topological constraints. We found indications that the α -effect even when restricted to the toroidal field greatly facilitates the development of small scales. Further investigations are however required to confirm that numerical instabilities are not significant.

We have identified two different modes of oscillations. The poloidal oscillations which depend on the advection of the toroidal field by poloidal flows, and the toroidal oscillations in which the toroidal field is created by the shearing toroidal motions.

With the α -effect, we have an extra time-scale α_T^{-1} added to the magnetohydrodynamics and hence a new class of local solutions different from Alfvén waves. We have shown that toroidal oscillations are well described by a particular kind of local solution near a neutral point. Both poloidal and toroidal oscillations transform an X-type neutral point into an O-point and thus inhibit current-sheet formation.

So far we have treated the α -effect as given. No underlying physical mechanism was considered. Making α a dynamical variable dependent on fields and flows could be an

interesting next step towards a better understanding of the relaxation processes.

We suggest that the investigation should now be developed in the following ways:

- 1) The parameter values of table 1 should be extended, particularly as regards smaller values of α , with a view to determining the critical value of α that prevents current-sheet formation.
- 2) Although we believe that boundary conditions are unimportant for the qualitative behaviour described, the computations should be repeated with flux conserving boundary conditions (i.e. $\frac{\partial B}{\partial r}|_{r=R} = 0$); also the effects of external driving should be incorporated, for example by choosing $\frac{\partial A}{\partial t}|_{r=R} \neq 0$.
- 3) The effects of non-zero α_P should be incorporated to see if this introduces any further qualitative changes.

Acknowledgements

One of us (K.B.) is very grateful to Dr M.K. Bevir and Dr C.G. Gimblett for many valuable discussions and the hospitality he enjoyed during his frequent visits to the Culham Laboratory. The work was carried out under Contract number EMR 470 M, U.K.A.E.A.

REFERENCES

- Arter, W. (1986) Local models of magnetohydrodynamics. *Culham report* TPN/86/5.
- Bajer, K. (1989) Flow kinematics and magnetostatic equilibria. Ph.D. Thesis. Cambridge University.
- Boozer, A.H. (1986) *J. Plasma Phys.* **35**, 133.
- Browning, P.K., Cunningham, G., Rusbridge, M.G. (1987) Spheromak research in Manchester. Proceedings of the International School of Plasma Physics, Varenna 1-11 Sept 1987, vol II.
- Gilbert, A.D., Sulem, P-L. (1990) On inverse cascades in alpha effect dynamos. *Geophys. Astrophys. Fluid Dynamics*, **51**, 243-261.
- Gimblett, C.G. & Watkins, M.L. (1975) 7th European Conf. on Controlled Fusion and Plasma Physics, Lausanne, Vol. I. 103.
- Gimblett, C.G. (1986) Private comm.
- Moffatt, H.K. (1978) *Magnetic Field Generation in Electrically Conducting Fluids*. Cambridge University Press.
- Moffatt, H.K. (1985) Magnetostatic equilibria and analogous Euler flows of arbitrarily complex topology. Part 1. Fundamentals. *J. Fluid Mech.*, **159**, 359-378.
- Moffatt, H.K. (1986) Magnetostatic equilibria and analogous Euler flows of arbitrarily complex topology. Part 2. Stability considerations. *J. Fluid Mech.*, **166**, 359-378.
- Priest, E.R. (1985) The magnetohydrodynamics of current sheets. *Rep. Prog. Phys.*, **48**, 955-1090.
- Roache, P.J. (1976) *Computational Fluid Dynamics*. Hermosa Publications.
- Soward, A.M., Priest, E.R. (1986) Magnetic field-line reconnection with jets. *J. Plasma Phys.*, **35**, part 2, 333-350.

Taylor J.B. (1974) Relaxation of toroidal plasma and generation of reverse magnetic fields. *Phys. Rev. Lett.* **33**, 1139-1141.

Weiss, N.O. (1989) Dynamo processes in stars. In G. Belvedere (ed.) *Accretion Disks and Magnetic Fields in Astrophysics*, pp. 11-29, Kluwer.

FIGURE CAPTIONS

- Figure 1. The contours of A for initial conditions and the equilibria towards which they relax when $\eta = \alpha_T = 0$:
- a) runs I, II: $S = 0.5$, $\alpha = 45^\circ$ - initial conditions;
 - b) run III: $S = 0$, $\alpha = 90^\circ$ - initial conditions;
- Figure 1. (ctd) The contours of A for initial conditions and the equilibria towards which they relax when $\eta = \alpha_T = 0$:
- c) runs I,II: $S = 0.5$, $\alpha = 45^\circ$ - final equilibrium;
 - d) run III: $S = 0$, $\alpha = 90^\circ$ - final equilibrium.
- Figure 2. a) The topology of the initial conditions when $S = 0$. When $\alpha_T = 0$ this topology is preserved.
- b) The change of topology at the initial stages of the evolution with $\alpha_T \neq 0$.
- Figure 3. The contours of A in run I. Time is written in the bottom corner.
- Figure 3. (ctd) The contours of A in run I. Time is written in the bottom corner.
- Figure 4. Run I
- a) The streamlines of the poloidal flow (Ψ -contours) at $t = 1.0$
 - b) The contours of the vertical field (B -contours) at $t = 1.0$
- Figure 4. (ctd) c) The field-lines of the poloidal field (A -contours) at $t = 1.36$
- d) The Ψ -contours at $t = 1.36$
- Figure 4. (ctd) e) The Ψ -contours at $t = 1.8$
- f) The B -contours at $t = 1.8$
- Figure 5. Run II
- a) The A -contours at $t = 1.2$
 - b) The A -contours at $t = 1.4$
- Figure 6. Run III
- a) B -contours at $t = 0.6$
 - b) B -contours at $t = 1.0$
- Figure 6. (ctd) c) B -contours at $t = 1.8$
- d) Ψ -contours at $t = 0.6$

Figure 6. (ctd) e) Ψ -contours at $t = 1.0$

f) Ψ -contours at $t = 1.8$

Figure 6. (ctd) g) V -contours at $t = 0.6$

h) V -contours at $t = 1.0$

Figure 6. (ctd) i) V -contours at $t = 1.8$

j) V -contours at $t = 2.6$

Figure 7. Local topology of the magnetic field.

Figure 8. The vertical velocity as a function of time in a numerical solution of the system (4.3) with the initial condition:

a) $A_1 = 0.1$, $A_2 = 1.0$, $B_1 = B_2 = 0$, $V = 0.01$;

b) $A_1 = 0.1$, $A_2 = 1.0$, $B_1 = B_2 = 0$, $V = 0.01$.

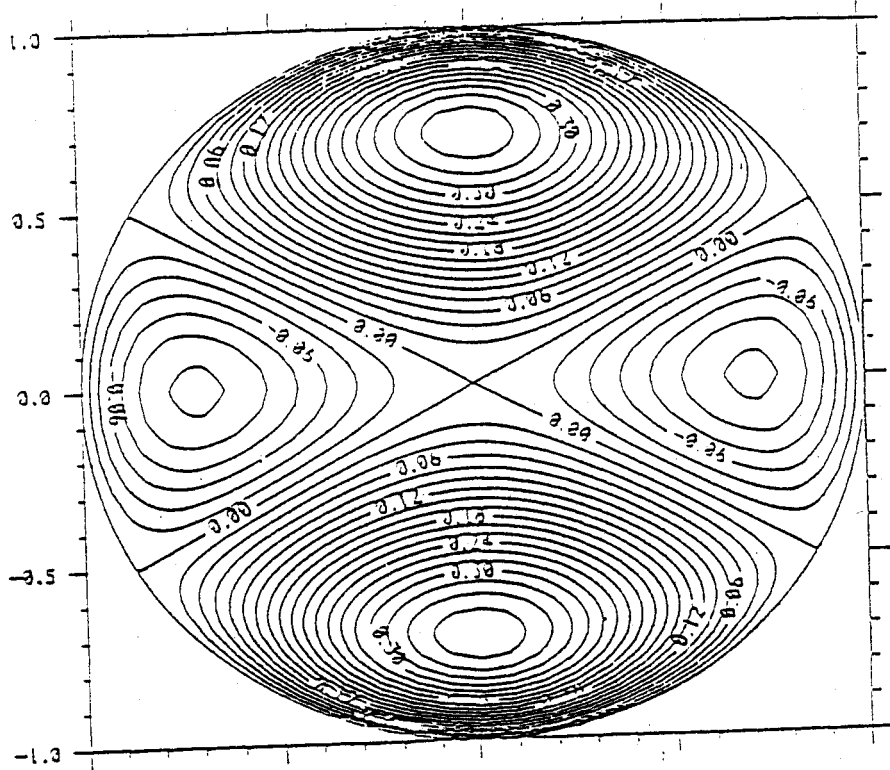
Figure 9. The parameter $f = A_1/(A_1 + A_2)$ as a function of time for the same solution as in fig. 8b.

Figure 10. The numerical solution of (4.3) with the initial condition $A_1 = 1.0$, $A_2 = 2.0$, $B_1 = 1.0$, $B_2 = -2.0$, $V = 0$.

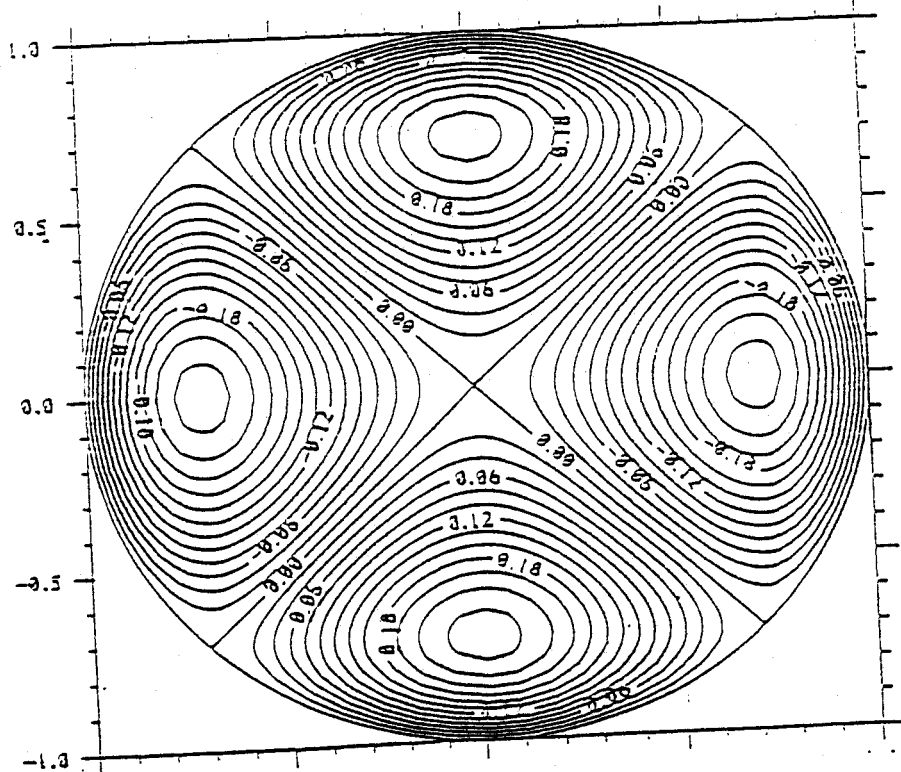
Table 1

	α_P	α_T	η	ν	S
RUN I	0	1	10^{-3}	1	0.5
RUN II	0	1	10^{-3}	10^{-3}	0.5
RUN III	0	1	10^{-3}	10^{-3}	0.0

Table 1. Parameter values in the three numerical simulations carried out.



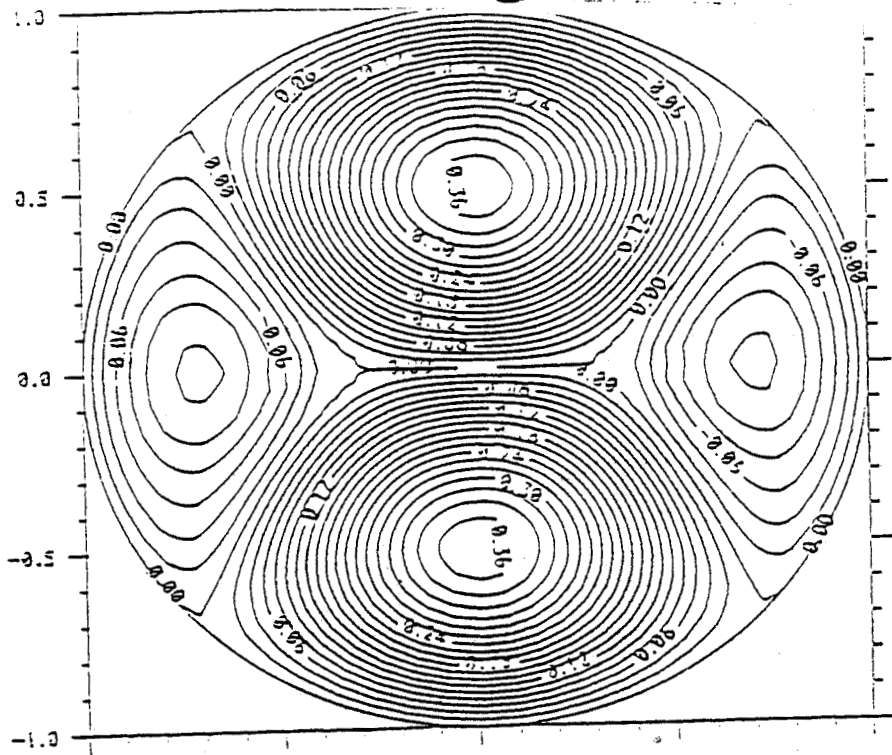
a)



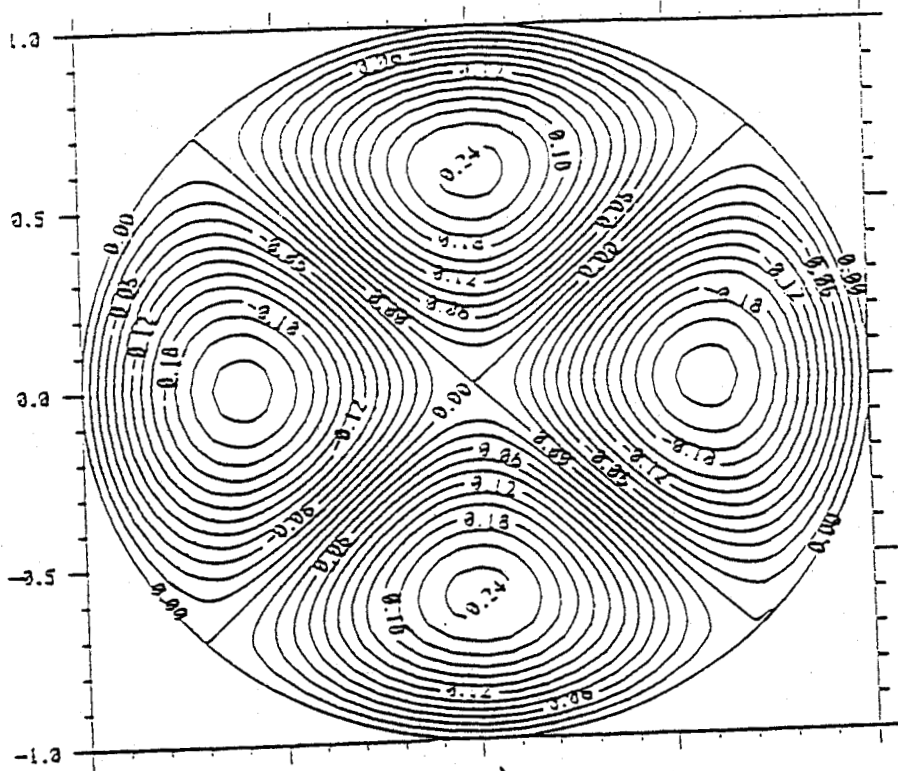
b)

Figure 1. The contours of A for initial conditions and the equilibria towards which they relax when $\eta = \alpha_T = 0$:

- a) runs I, II: $S = 0.5$, $\alpha = 45^\circ$ - initial conditions;
- b) run III: $S = 0$, $\alpha = 90^\circ$ - initial conditions;



c)

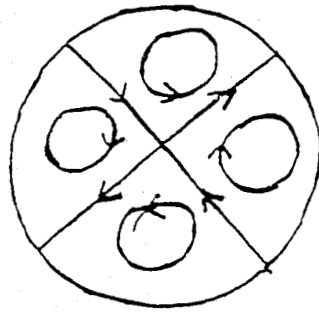


d)

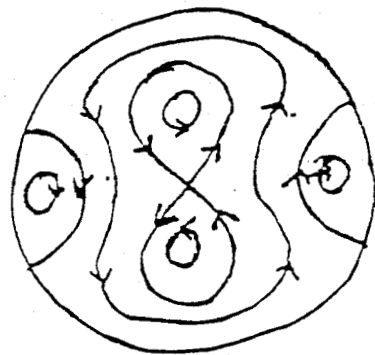
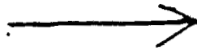
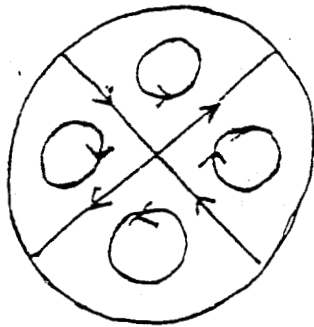
Figure 1. (ctd) The contours of A for initial conditions and the equilibria towards which they relax when $\eta = \alpha_T = 0$:

c) runs I,II: $S = 0.5$, $\alpha = 45^\circ$ - final equilibrium;

d) run III: $S = 0$, $\alpha = 90^\circ$ - final equilibrium.



a)

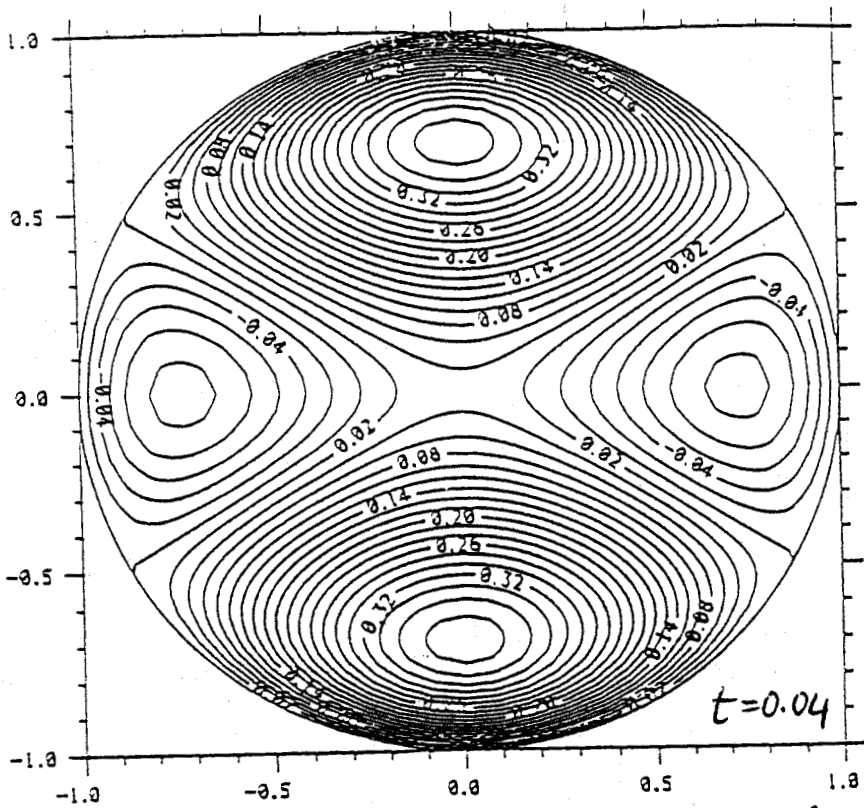


b)

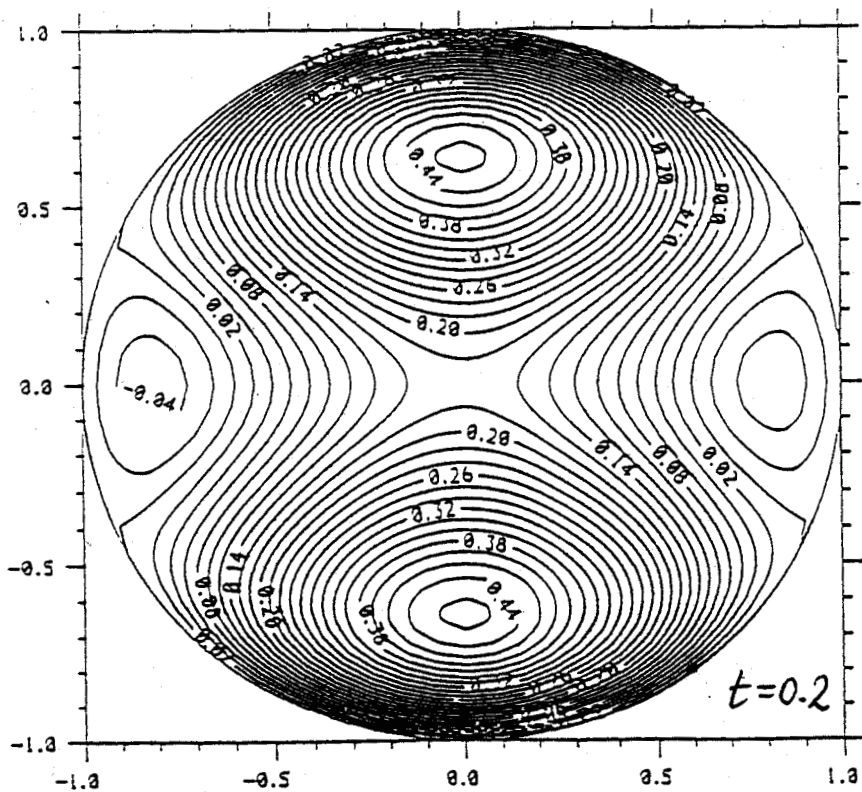
Figure 2.

a) The topology of the initial conditions when $S = 0$. When $\alpha_T = 0$ this top is preserved.

b) The change of topology at the initial stages of the evolution with $\alpha_T \neq 0$.



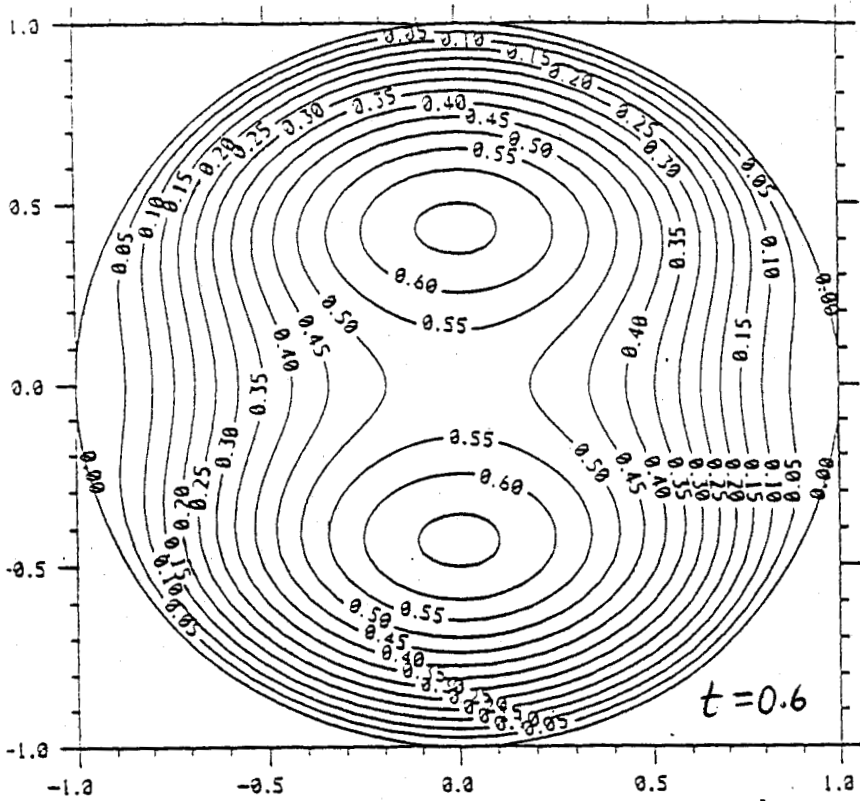
a)



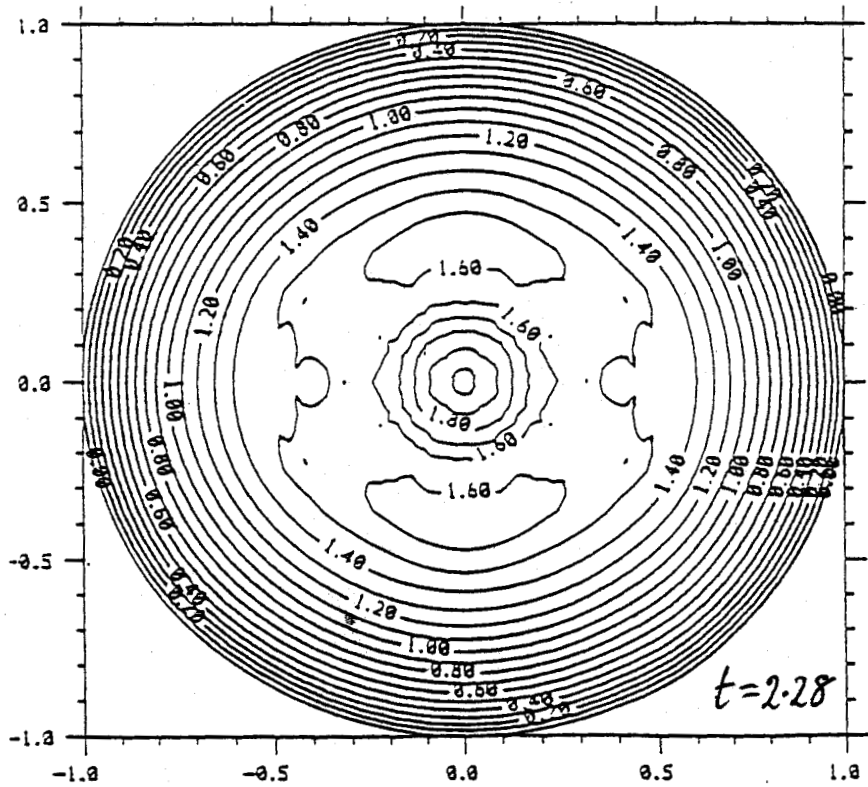
b)

Figure 3.

The contours of A in run I. Time is written in the bottom corner.

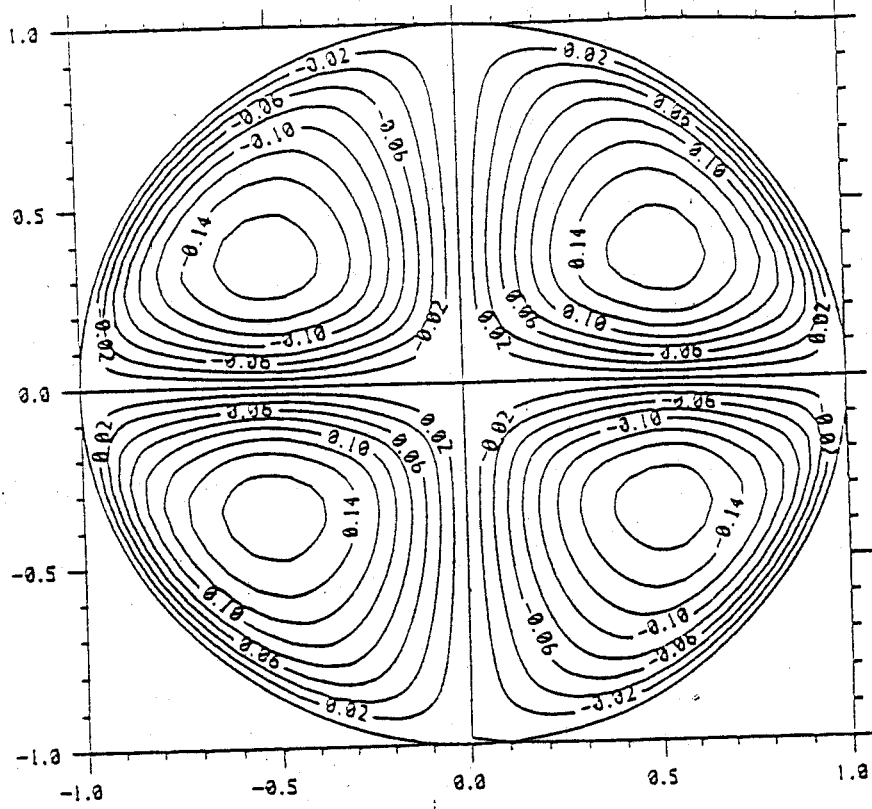


c)

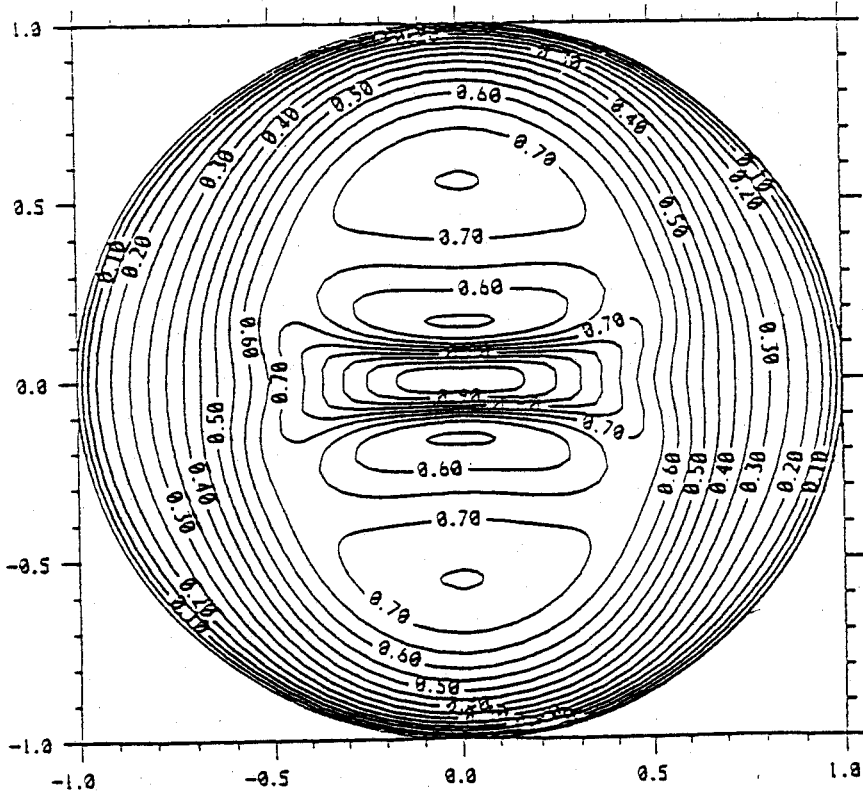


d)

Figure 3. (ctd) The contours of A in run I. Time is written in the bottom corner.



a)



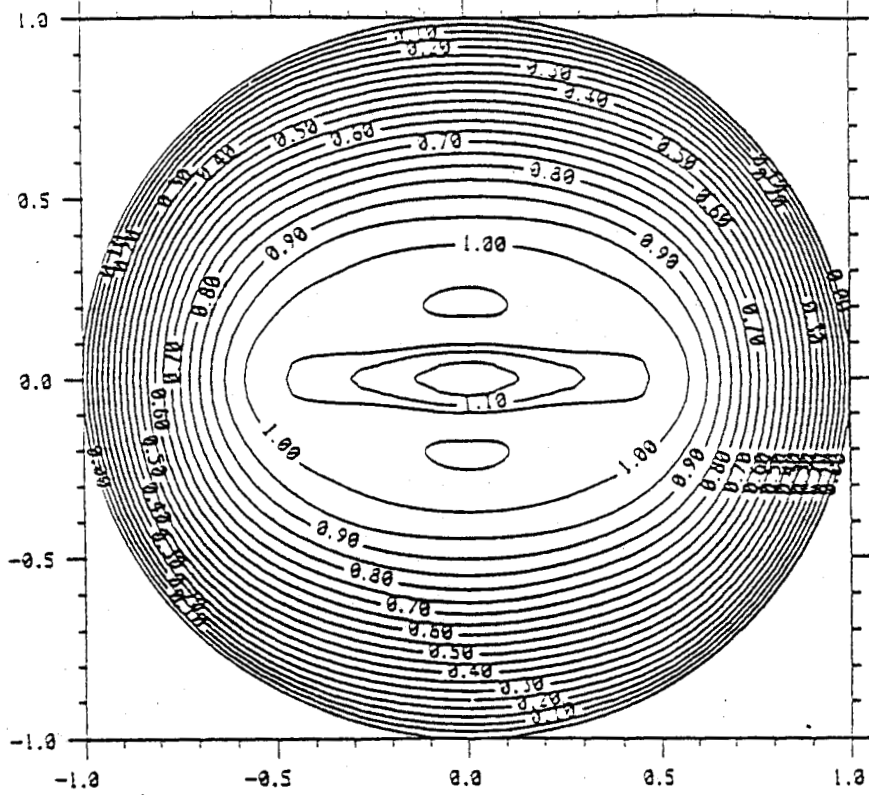
b)

Figure 4.

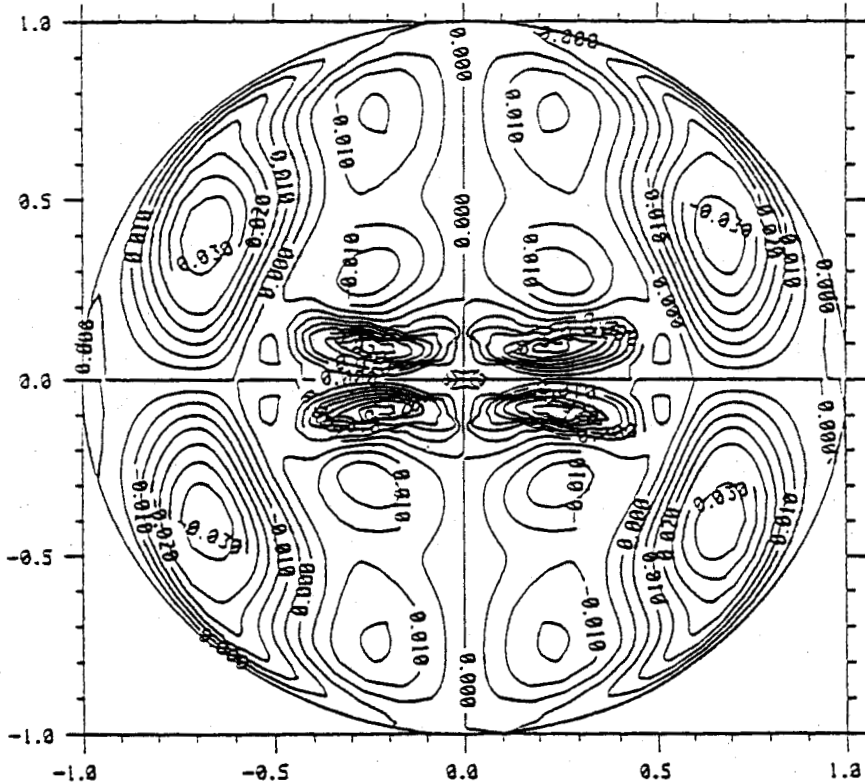
Run I

a) The streamlines of the poloidal flow (Ψ -contours) at $t = 1.0$

b) The contours of the vertical field (B -contours) at $t = 1.0$

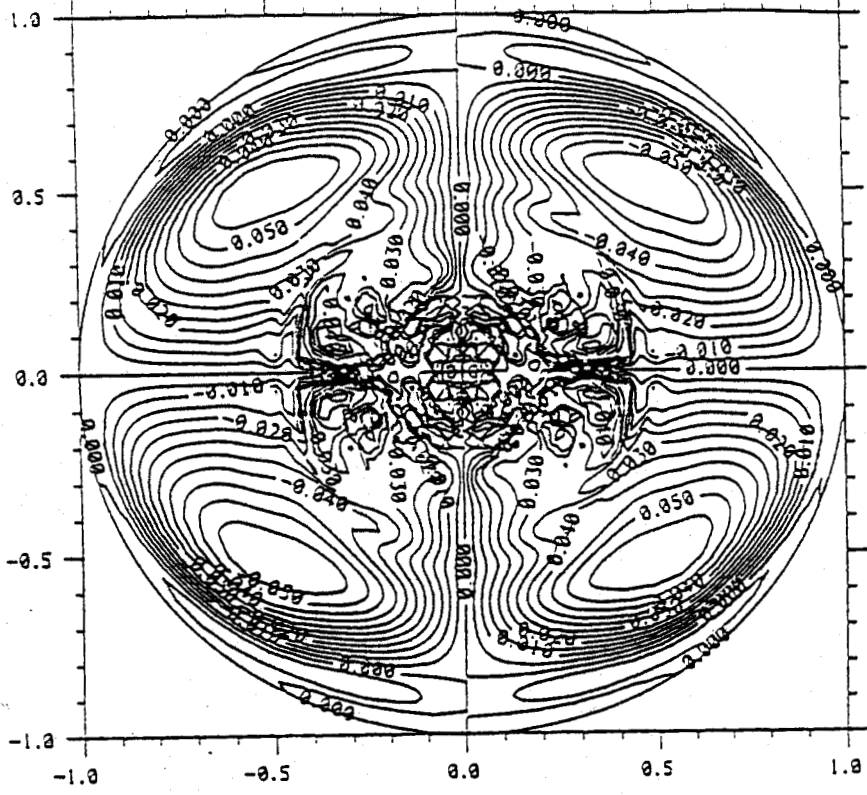


c)

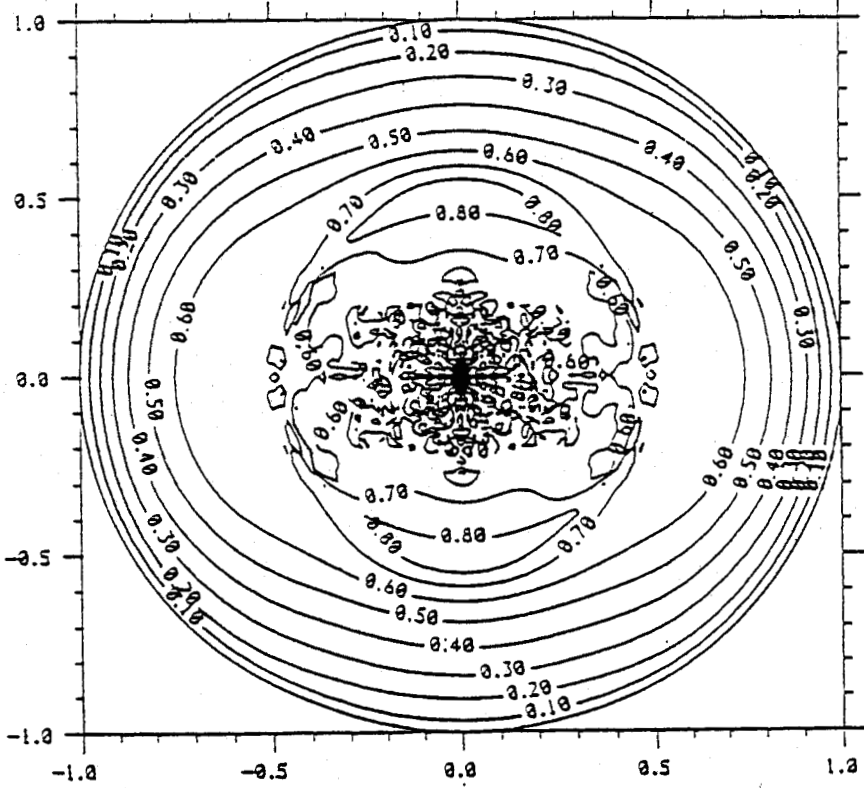


d)

Figure 4. (ctd) c) The field-lines of the poloidal field (A -contours) at $t = 1.36$
 d) The Ψ -contours at $t = 1.36$



e)



f)

Figure 4. (ctd) e) The Ψ -contours at $t = 1.8$
 f) The B -contours at $t = 1.8$

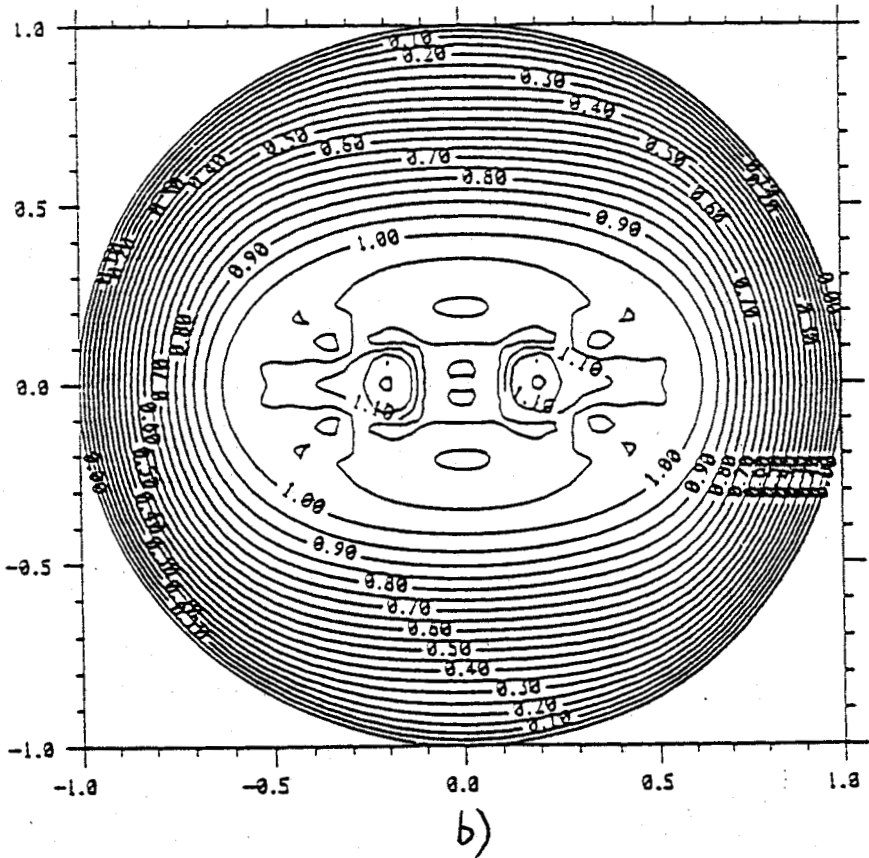
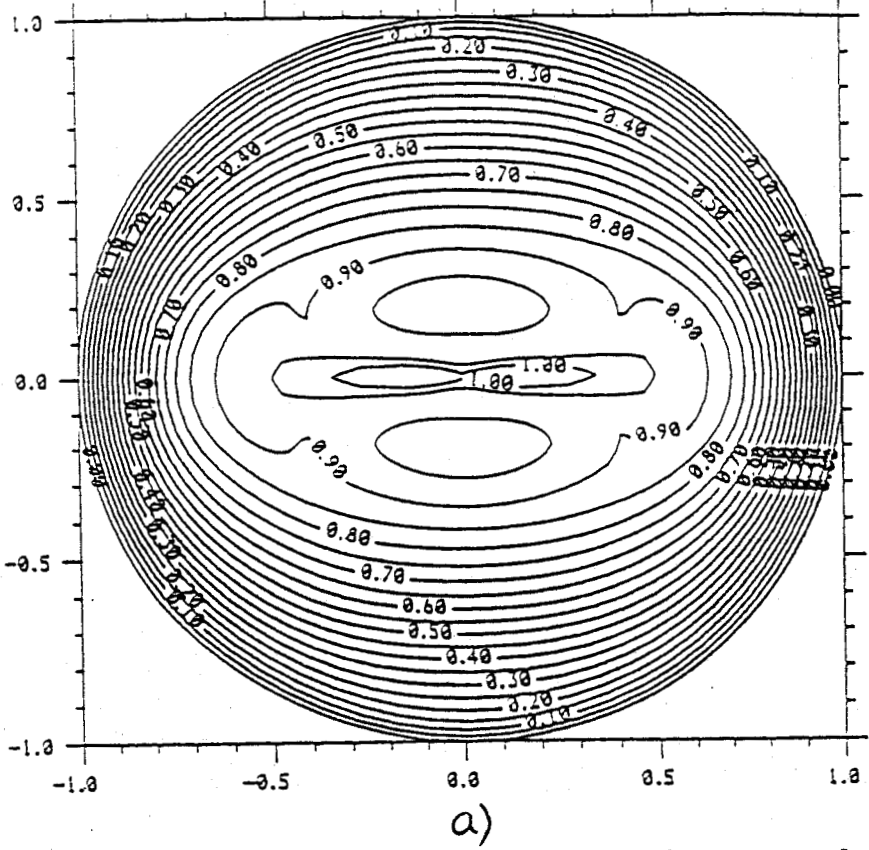
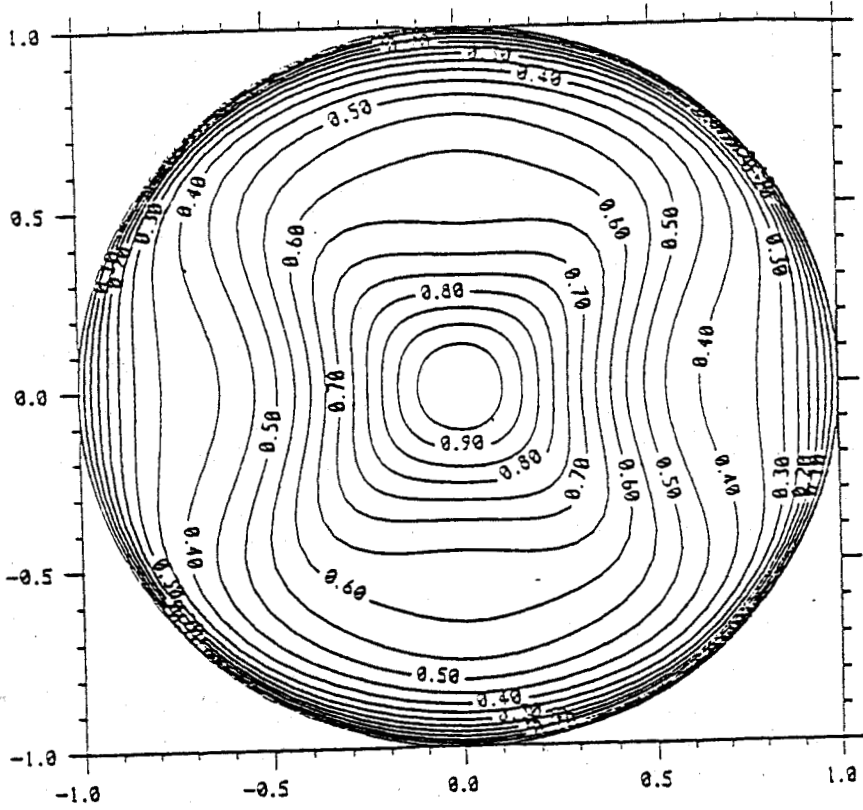
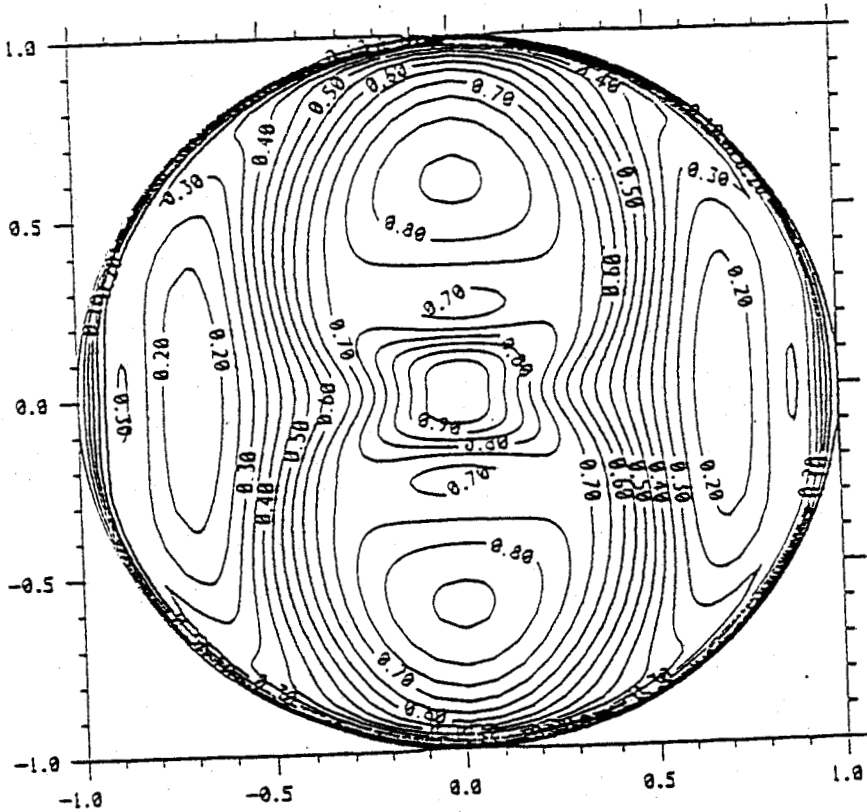


Figure 5. Run II
 a) The A -contours at $t = 1.2$
 b) The A -contours at $t = 1.4$



a)



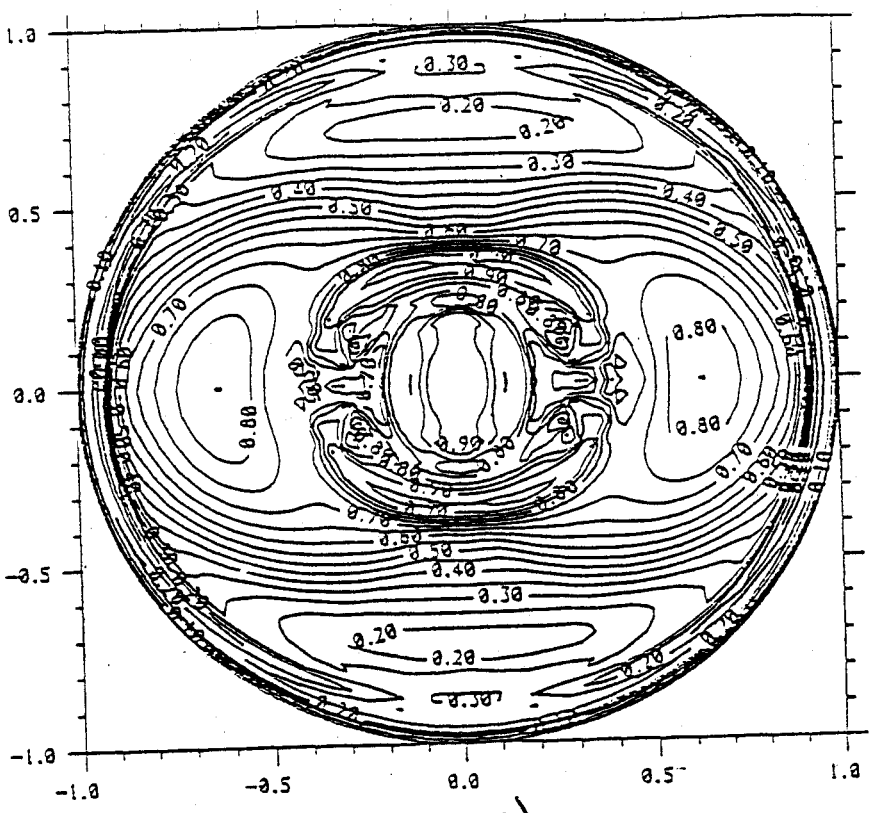
b)

Figure 6.

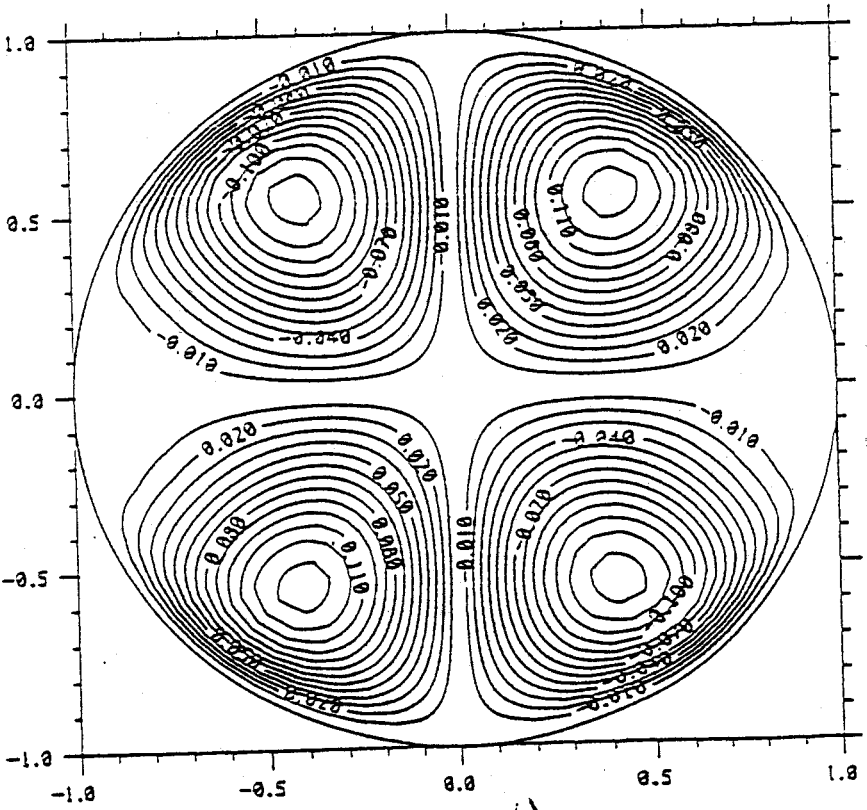
Run III

a) B -contours at $t = 0.6$

b) B -contours at $t = 1.0$



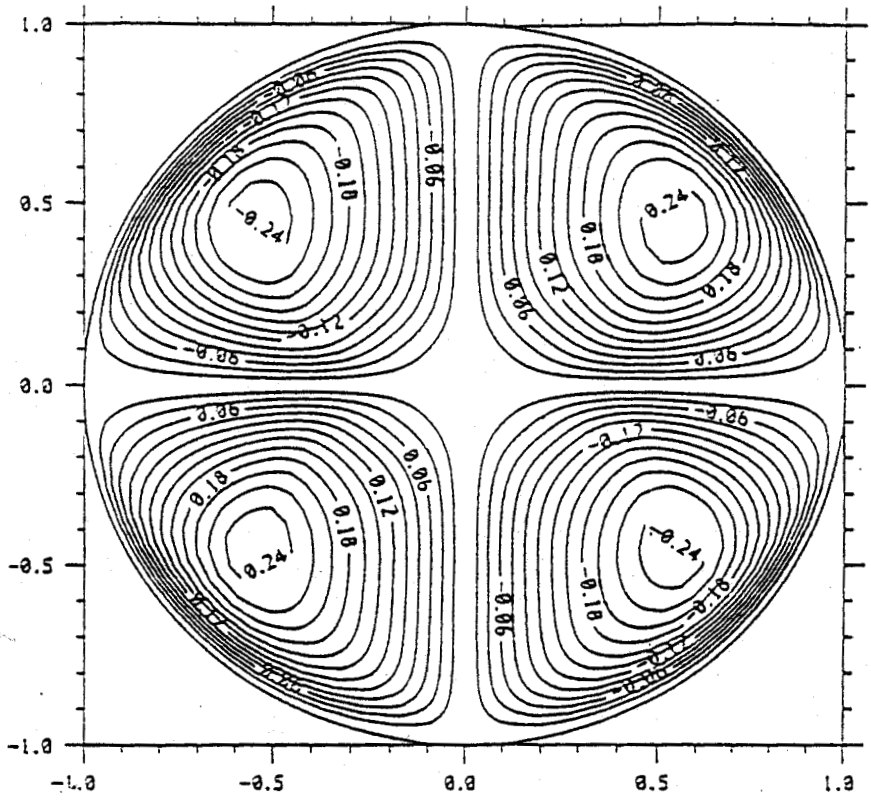
c)



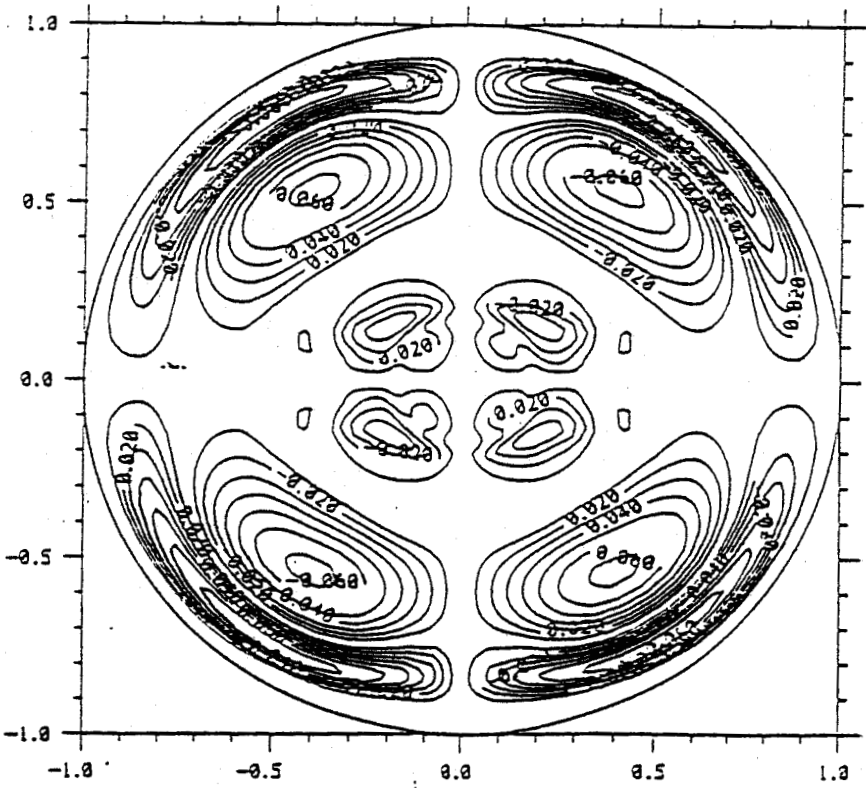
d)

Figure 6. (ctd) c) B -contours at $t = 1.8$

d) Ψ -contours at $t = 0.6$



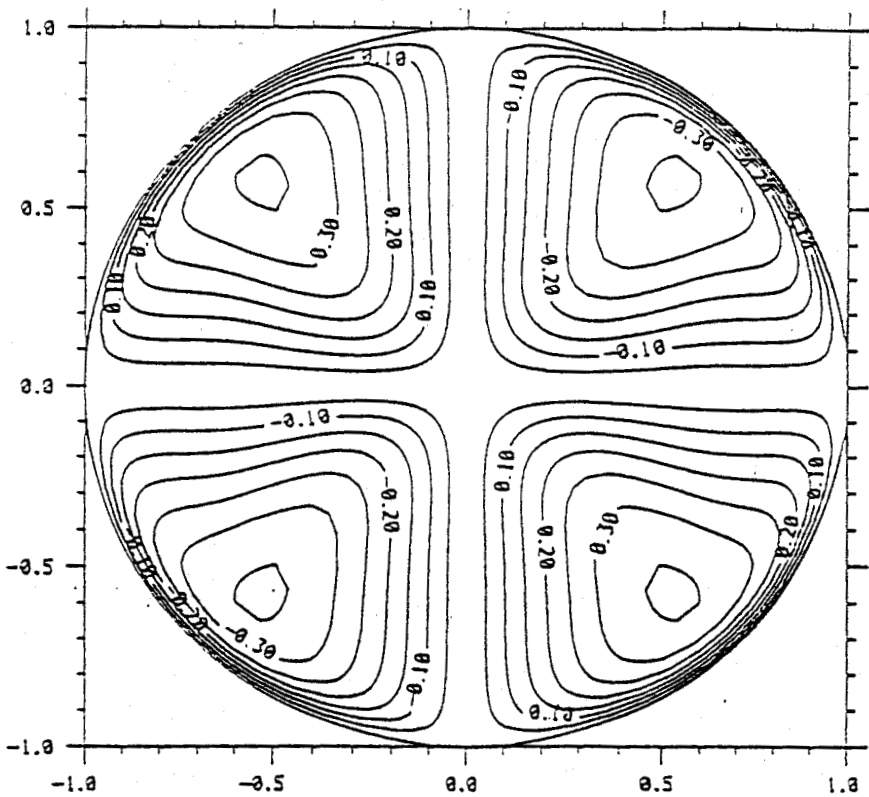
e)



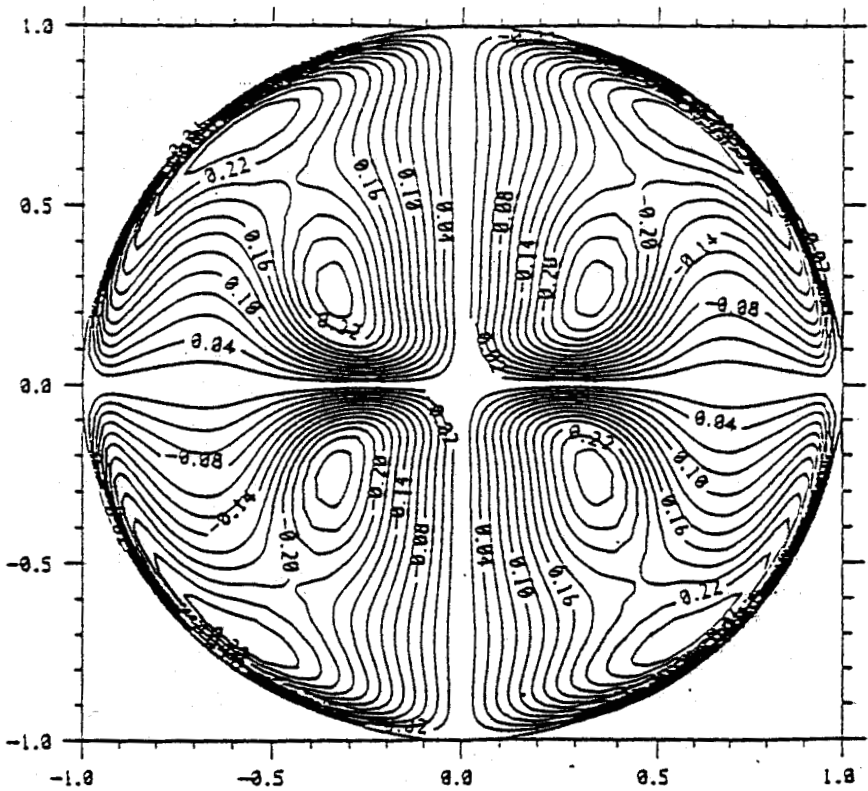
f)

Figure 6. (ctd) e) Ψ -contours at $t = 1.0$

f) Ψ -contours at $t = 1.8$



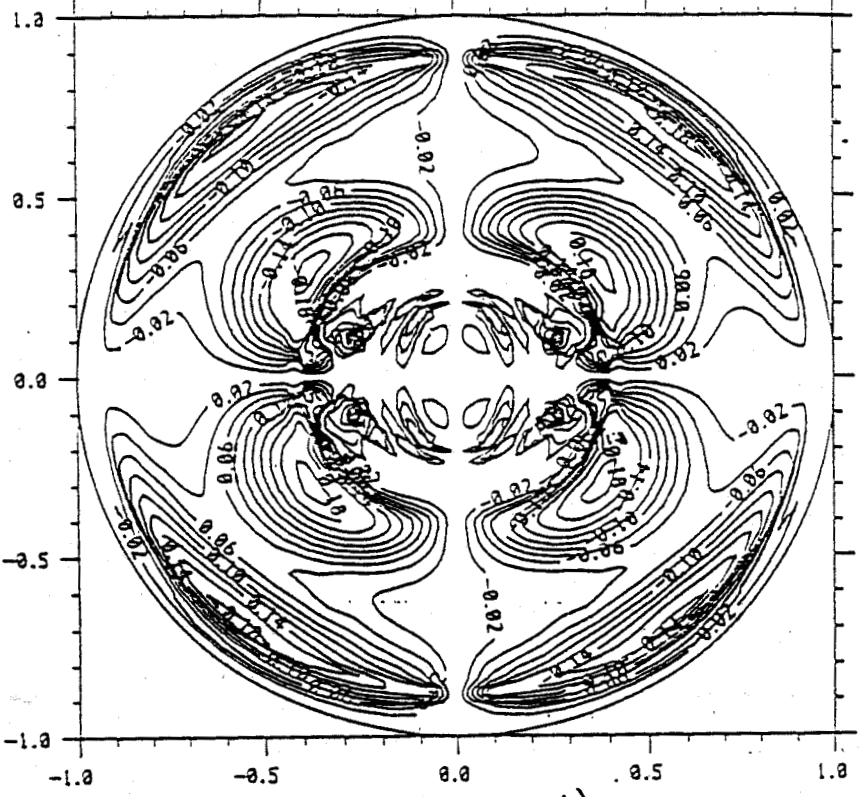
g)



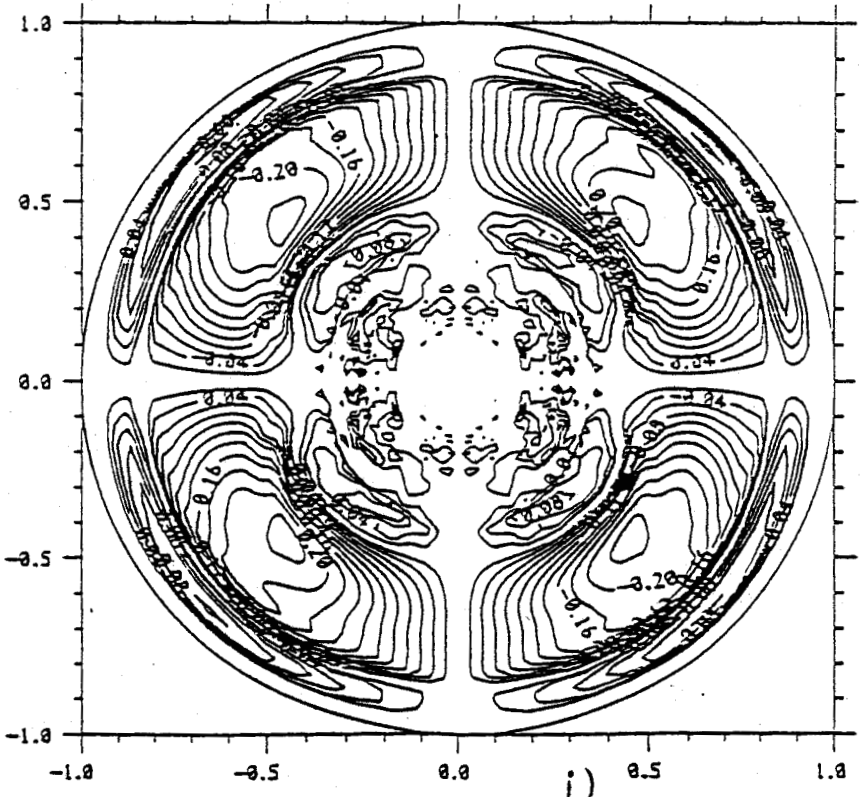
h)

Figure 6. (ctd) g) V -contours at $t = 0.6$

h) V -contours at $t = 1.0$

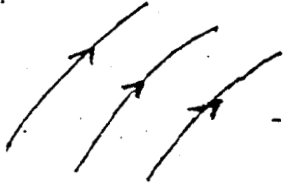


i)

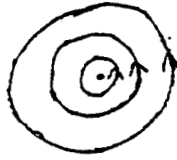


j)

Figure 6. (ctd) i) V -contours at $t = 1.8$
 j) V -contours at $t = 2.6$



a) $B_0, A_1, A_2 \neq 0$



b) $A_1 = A_2 = B_0 = 0$

Figure 7. Local topology of the magnetic field.

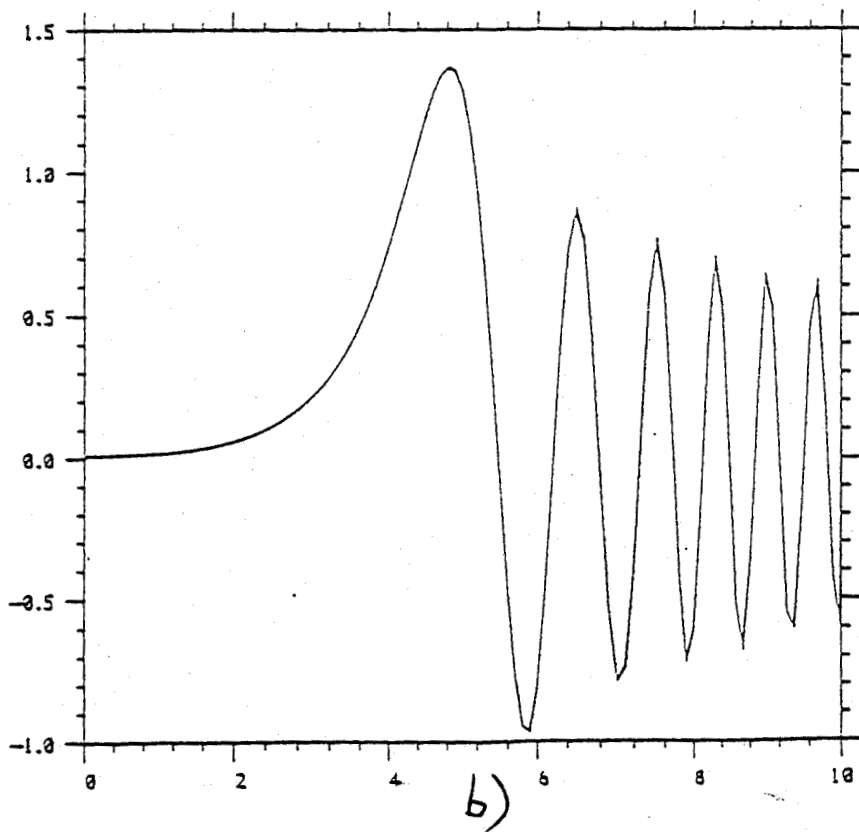
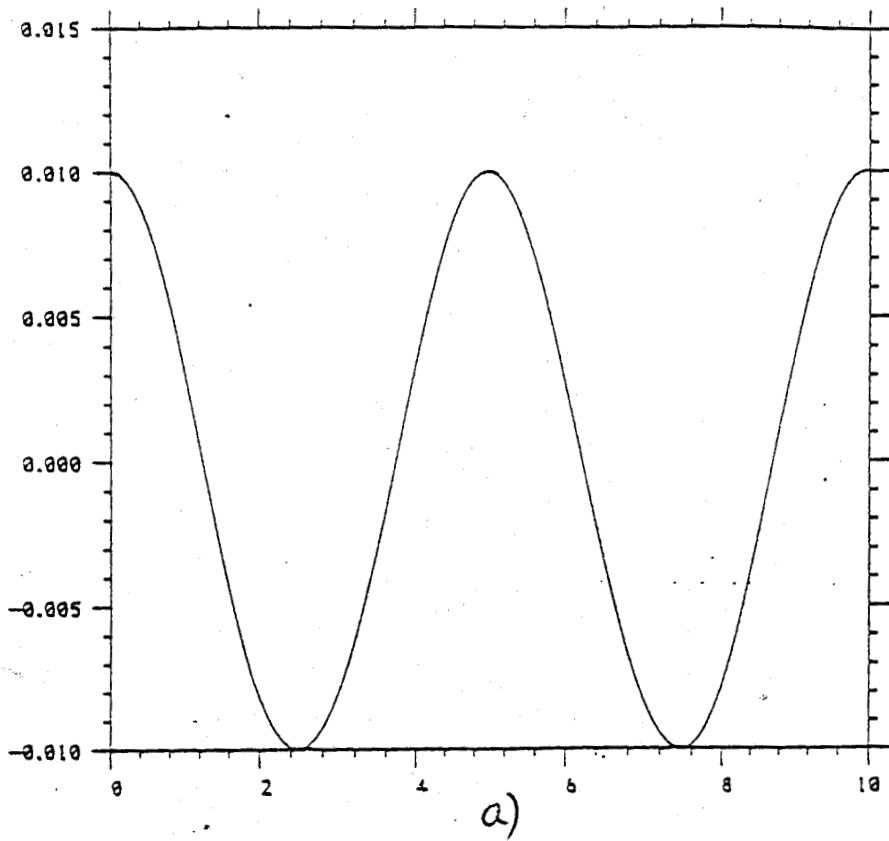


Figure 8.

The vertical velocity as a function of time in a numerical solution of the system (4.3) with the initial condition:

a) $A_1 = 0.1, A_2 = 1.0, B_1 = B_2 = 0, V = 0.01$;

b) $A_1 = 0.1, A_2 = 1.0, B_1 = B_2 = 0, V = 0.01$.

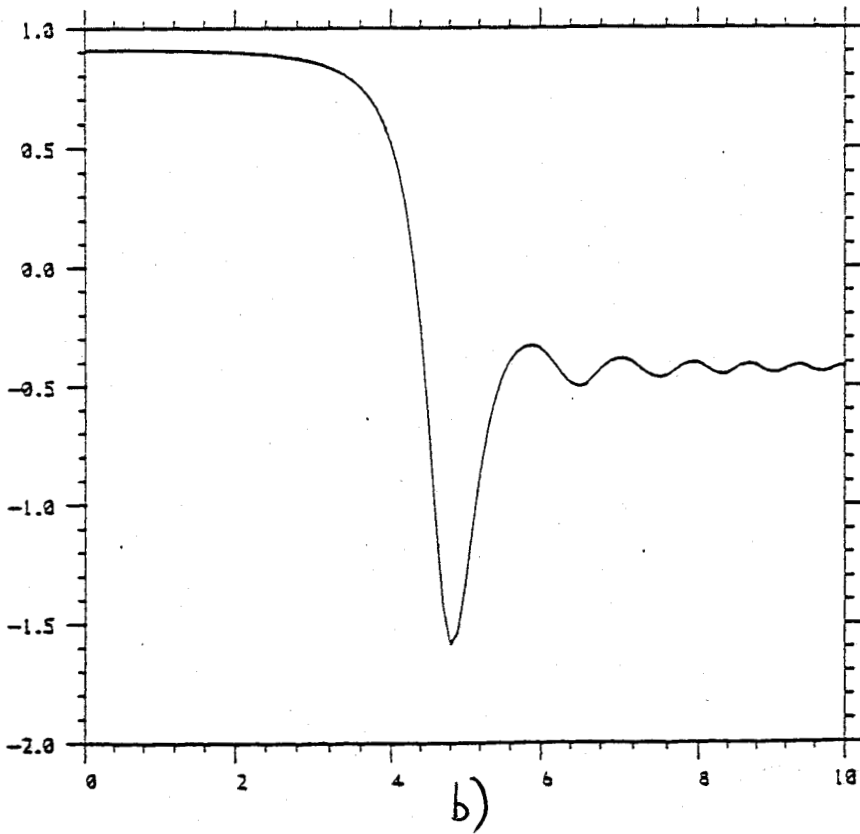
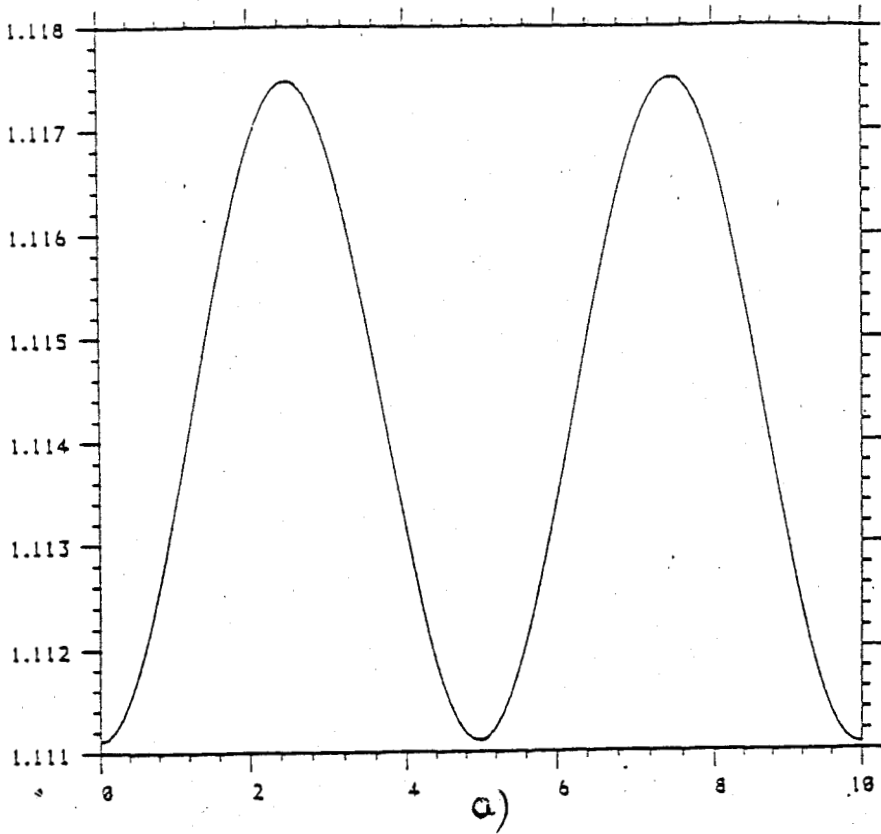


Figure 9. The parameter $f = A_1 / (A_1 + A_2)$ as a function of time for the same solution as in fig. 8.

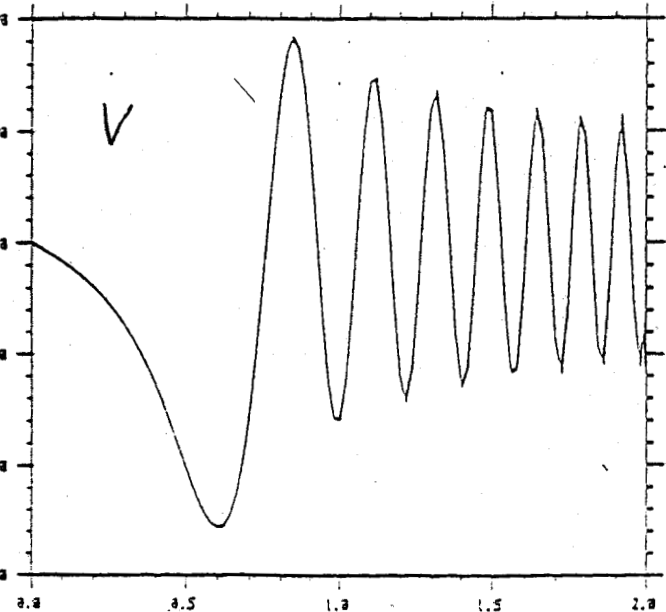
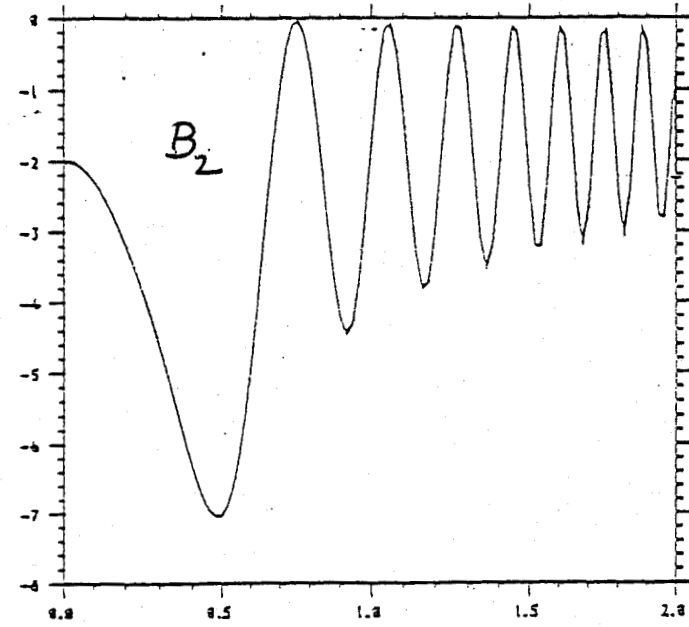
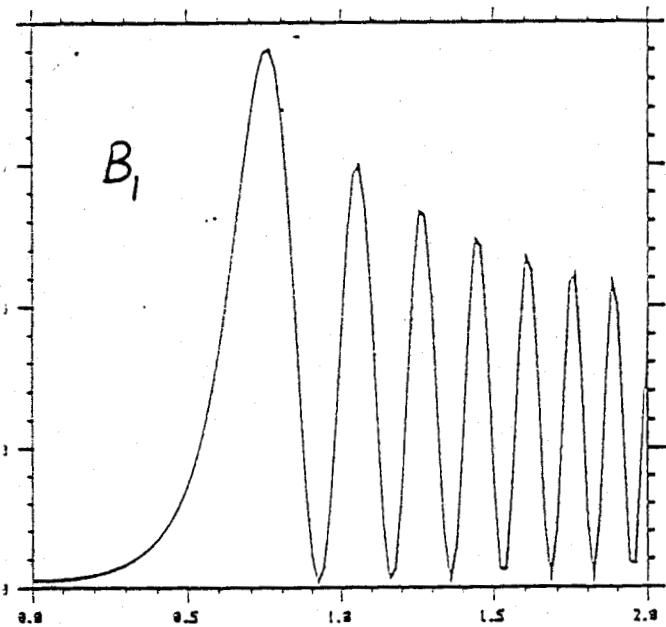
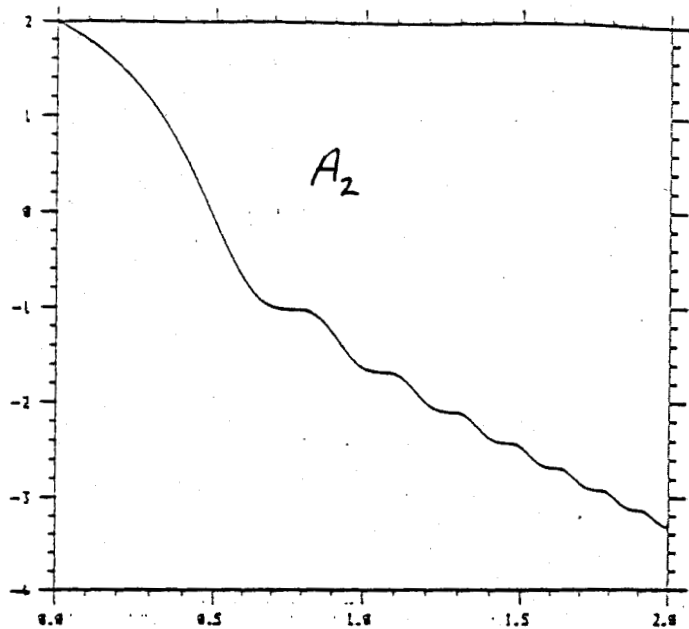
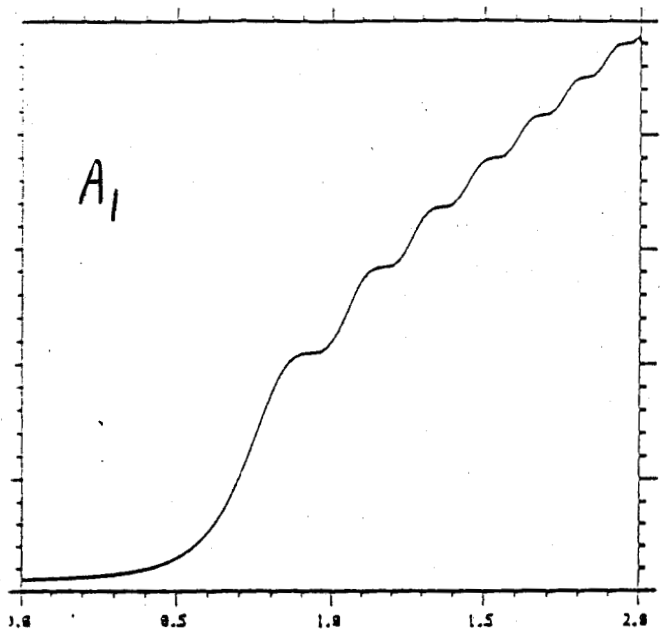


Figure 10. The numerical solution of (4.3) with the initial condition $A_1=1.0$, $A_2=2.0$, $B_1=1.0$, $B_2=-2.0$, $V=0$.